Empirical evidence for stability of the 405-kiloyear Jupiter–Venus eccentricity cycle over hundreds of millions of years

Dennis V. Kent[a,b,1], Paul E. Olsen[b], Cornelia Rasmussen[c], Christopher Lepre[a,b], Roland Mundil[d], Randall B. Irmis[c,e], George E. Gehrels[f], Dominique Giesler[f], John W. Geissman[g], and William G. Parker[h]

[a]Department of Earth and Planetary Sciences, Rutgers University, Piscataway, NJ 08854; [b]Lamont–Doherty Earth Observatory, Columbia University, Palisades, NY 10964; [c]Department of Geology and Geophysics, University of Utah, Salt Lake City, UT 84112; [d]Berkeley Geochronology Center, Berkeley, CA 94709; [e]Natural History Museum of Utah, University of Utah, Salt Lake City, UT 84108; [f]Department of Geosciences, University of Arizona, Tucson, AZ 85721; [g]Department of Geosciences, University of Texas at Dallas, Richardson, TX 75080; and [h]Division of Science and Resource Management, Petrified Forest National Park, Petrified Forest, AZ 86028

Edited by Lisa Tauxe, University of California, San Diego, La Jolla, CA, and approved April 6, 2018 (received for review January 16, 2018)

The Newark–Hartford astrochronostratigraphic polarity timescale (APTS) was developed using a theoretically constant 405-kiloyear eccentricity cycle linked to gravitational interactions with Jupiter–Venus as a tuning target and provides a major timing calibration for about 30 million years of Late Triassic and earliest Jurassic time. While the 405-ky cycle is both unimodal and the most metronomic of the major orbital cycles thought to pace Earth's climate in numerical solutions, there has been little empirical confirmation of that behavior, especially back before the limits of orbital solutions at about 50 million years before present. Moreover, the APTS is anchored only at its younger end by U–Pb zircon dates at 201.6 million years before present and could even be missing a number of 405-ky cycles. To test the validity of the dangling APTS and orbital periodicities, we recovered a diagnostic magnetic polarity sequence in the volcaniclastic-bearing Chinle Formation in a scientific drill core from Petrified Forest National Park (Arizona) that provides an unambiguous correlation to the APTS. New high precision U–Pb detrital zircon dates from the core are indistinguishable from ages predicted by the APTS back to 215 million years before present. The agreement shows that the APTS is continuous and supports a stable 405-kiloyear cycle well beyond theoretical solutions. The validated Newark–Hartford APTS can be used as a robust framework to help differentiate provinciality from global temporal patterns in the ecological rise of early dinosaurs in the Late Triassic, amongst other problems.

magnetostratigraphy | geochronology | astrochronology | Milankovitch | Triassic

The 27-My Newark–Hartford astrochronostratigraphic polarity timescale (APTS) (1) is one of the longest continuous APTS segments presently available and calibrates much of the Late Triassic and earliest Jurassic geologic timescale. It relies on the geomagnetic polarity and cycle stratigraphies of over 6,900 m of coring in the Newark basin (2–4) and an overlapping 2,500-m-thick outcrop section in the nearby Hartford basin (5), both in eastern North America. The composite continental record is paced by 66 McLaughlin lithologic cycles spanning 27 My of the Norian and Rhaetian of the Late Triassic and Hettangian and Sinemurian of the Early Jurassic, reflecting the response of climate to the long astronomical eccentricity variation with a presumed 405-ky period. The 405-ky period cycle is related to the gravitational interaction of Jupiter and Venus (g2–g5 cycle) and is the prominent and most stable term in the approximation of eccentricity of Earth's orbital variations on geologic timescales despite chaotic behavior of the Solar System (6). The record also encompasses 51 Poisson-distributed geomagnetic polarity intervals (with an additional 15 polarity intervals in the fluvial noncyclic sediments toward the base of the section, which by extrapolation of sediment accumulation rates extend the record an additional ∼6 My into the Carnian), providing a template for global correlation. However, the astronomically paced polarity sequence is anchored at essentially only one level. High-precision U–Pb zircon dates in lavas and intrusions of the Central Atlantic Magmatic Province (CAMP), which are clustered in close spatiotemporal proximity to the Triassic–Jurassic boundary (7), were collapsed to a calibration age of 201.6 Ma for the onset of Chron E23r close to the base of a McLaughlin cycle (Ecc_{405}: k = 498.25, where k is the inferred number of 405-ky eccentricity cycles projected back from the most recent maximum at 0.216 million years ago as k = 1), which immediately underlies the oldest CAMP basalts. In the absence of other directly dated horizons, the APTS relies on the assumption of a continuous section with no substantial hiatus(es) in deposition of these continental sediments, which would potentially result in one or more unrecorded 405-ky cycles. The specific timing of the APTS is also dependent on the untested reliability at this distant age range of the 405-ky cycle.

The developing APTS has been successfully used for global correlations in marine and nonmarine facies (e.g., refs. 8 and 9; see ref. 1). Nevertheless, there have been persistent suggestions made largely on the basis of nonmarine biostratigraphic correlations that several million years of Rhaetian (latest Triassic) time are missing in a cryptic unconformity that supposedly occurs just above Chron E23r in the Newark Supergroup basins (e.g., refs. 10 and 11). If true, this would have consequences of comparable magnitude in the timing of events based on anchoring

Significance

Rhythmic climate cycles of various assumed frequencies recorded in sedimentary archives are increasingly used to construct a continuous geologic timescale. However, the age range of valid theoretical orbital solutions is limited to only the past 50 million years. New U–Pb zircon dates from the Chinle Formation tied using magnetostratigraphy to the Newark–Hartford astrochronostratigraphic polarity timescale provide empirical confirmation that the unimodal 405-kiloyear orbital eccentricity cycle reliably paces Earth's climate back to at least 215 million years ago, well back in the Late Triassic Period.

Author contributions: D.V.K. and P.E.O. designed research; D.V.K., P.E.O., C.R., C.L., R.M., R.B.I., J.W.G., and W.G.P. performed research; R.B.I. and J.W.G. assisted in recovery and description of core; R.B.I. and W.G.P. provided regional geologic context; W.G.P. assisted in providing access to the Petrified Forest National Park; D.V.K., C.R., R.M., G.E.G., and D.G. analyzed data; and D.V.K., P.E.O., and R.M. wrote the paper.

The authors declare no conflict of interest.

This article is a PNAS Direct Submission.

[1]To whom correspondence should be addressed. Email: dvk@rutgers.edu.

This article contains supporting information online at www.pnas.org/lookup/suppl/doi:10.1073/pnas.1800891115/-/DCSupplemental.

the astrochronology below the alleged cryptic unconformity to the U–Pb-dated CAMP lavas above it. Therefore, a test is needed of the conjoined assumptions of stratigraphic continuity and the 405-ky periodicity for the long eccentricity cycle that are implicit in the construction of the Newark–Hartford APTS.

The Late Triassic-age Chinle Formation (Fm.) of the American Southwest (Fig. 1*A*) consists of fluvial and minor lacustrine facies interfingered with paleosols and, importantly for the task at hand, has numerous sandstone horizons with volcaniclastic detritus containing detrital zircons amenable for U–Pb dating (12). The Black Forest Bed (BFB) within the Petrified Forest Member (Mb.) of the Chinle Fm. at Chinde Point in the northern sector of Petrified Forest National Park (PFNP) was the first unit to be successfully U–Pb zircon dated in the PFNP section (13). Recent high-precision U–Pb zircon dating of the BFB (12) made it an attractive target for calibration of the APTS. Sampling of outcrop sections demonstrated the feasibility of obtaining a magnetostratigraphy (14) even though revised long-distance lithostratigraphic correlations of the Sonsela Mb. of the Chinle Fm. (15) indicate that there may be a large gap in the composite magnetostratigraphic section. A main scientific objective of the inaugural drilling effort of the Colorado Plateau Coring Project (16) at PFNP (core CPCP-PFNP-13-1A; henceforth PFNP-1A) (Fig. 1*B*) was to obtain a magnetostratigraphic sequence directly supported by high-precision U–Pb detrital zircon dates for the Chinle Fm. with unequivocal superposition and a diagnostic polarity signature for correlation to the APTS. Here, we report on paleomagnetic and geochronologic results from the upper ~280 m of the 519-m-long core recovering a section of the Chinle Fm. down from the lower Owl Rock Mb. to the Mesa Redondo Mb., the Moenkopi Fm. and the uppermost Coconino Sandstone (Fig. 1*B*).

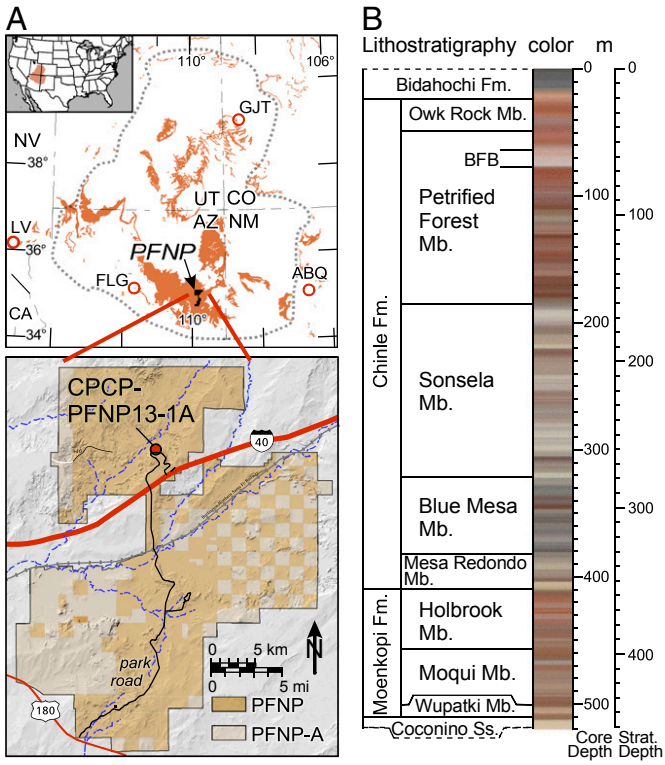

Fig. 1. Geographic location and stratigraphy of scientific drill core CPCP-PFNP-13-1A in Petrified Forest National Park (Arizona). (*A*) Nested maps showing location of core PFNP-1A in Petrified Forest National Park (PFNP) on the Colorado Plateau in western North America. (*B*) Stratigraphic log of continuously cored section of the Bidahochi, Chinle, Moenkopi, and Coconino formations recovered in core PFNP-1A is shown with lithostratigraphic unit names (38), and the predominant color of the sediments from a digitally smoothed, enhanced color profile based on spectrophotometer data provided by LacCore (courtesy of Anders Noren, University of Minnesota, Minneapolis). Core length (in meters core depth) was converted to stratigraphic thickness (in meters stratigraphic depth) assuming flat-lying strata with core drilled 30° from vertical, and hence stratigraphic thickness is 86.6% of core length. ABQ, Albuquerque; AZ, Arizona; CA, California; CO, Colorado; FLG, Flagstaff; GJT, Grand Junction; LV, Las Vegas; NM, New Mexico; NV, Nevada; PFNP, Petrified Forest National Park; PFNP-A, Private or State Trust land; PFNP-CPCP13-1A, core site at Chinde Point.

Results

Following the procedures described in *Materials and Methods* and *SI Appendix*, characteristic remanent magnetization (ChRM) directions were successfully isolated in 132 of the 174 oriented subsamples extracted from ~24–278 meters core depth (mcd) [~21–248 meters stratigraphic depth (msd)] encompassing the lower Owl Rock Mb., the entire Petrified Forest Mb. including the BFB, and down into the middle part of the Sonsela Mb. The ChRM direction for each sample was converted to a virtual geomagnetic pole (VGP) whose latitude with respect to the 210-Ma reference (north) paleopole (17), referred to as rVGP latitude, is used to designate polarity. A plot of rVGP latitudes with depth in core PFNP-1A shows a series of magnetic polarity zones that are designated from the top down as PF1r (*partim*), PF2n, PF2r, PF3n, PF3r (with a thin normal polarity interval, PF3r.1n), PF4n, PF4r, and PF5n (*partim*) (Fig. 2). The paleomagnetic signature of sediments of the Owl Rock Mb. from immediately below the erosional unconformity with the late Cenozoic Bidahochi Fm. (not sampled) at 20.6 msd to around 35 msd is erratic, which we attribute to complications during coring and recovery of this shallow and poorly indurated material. The coherence of the polarity data improves sufficiently down core to establish that the lowermost Owl Rock Mb. is in a reverse polarity magnetozone (PF1r) that extends down to a normal magnetozone PF2n (41.1–48.0 msd) straddling the contact with the Petrified Forest Mb. at 41.7 msd. The underlying reverse polarity magnetozone PF2r (48.0–64.5 msd) is sparsely documented because the pale-colored cross-bedded sands and silts of the BFB (~55.5–66.9 msd) that dominate this interval are poor paleomagnetic recorders, with only 3 out of 17 samples providing acceptable results. Finer-grained red lithologies are more common in the underlying part of the Petrified Forest Mb. and record substantial evidence of a thick (64.5–125.4 msd) normal polarity magnetozone (PF3n), a modestly thick (125.4–153.9 msd) reverse magnetozone (PF3r) that includes a thin (144.5–149.5 msd) normal polarity interval in its lower part, and a normal magnetozone (PF4n; 153.9–187.3 msd) that extends below the contact with the Sonsela Mb. (160.3 msd). The generally coarser and less red lithologies of the Sonsela Mb. proved more difficult for obtaining a coherent paleomagnetic signature. The available data delineate reverse polarity magnetozone PF4r from 187.3 to 215.7 msd and normal polarity magnetozone PF5n from 215.7 msd to the lowest sample with acceptable data in this suite at 240.8 msd. There are also three putative (one-sample) polarity magnetozones of uncertain origin (e.g., inverted samples?) that are not interpreted further.

Given the overall lithostratigraphic, biostratigraphic, and geochronologic framework of the upper Chinle Fm (12, 18), the most plausible correlation of the local magnetozones (PF1r to PF5n, youngest to oldest) equates them to chrons E17r to E14n (younger to older) of the APTS, spanning ~209.5–215.5 Ma (Fig. 2).

The BFB is a distinctive white tuffaceous crevasse-splay sandstone (13, 19) that can be more than 10 m thick. It occurs within the upper part of the mostly red Petrified Forest Mb. and can be readily traced in outcrops throughout the northern part of the PFNP, including Chinde Point. A ~50-m-thick normal polarity interval equivalent to magnetozone PF3n was also found just below the BFB in outcrop (14) but was miscorrelated to Chron E15n, although the thin normal within the underlying reverse polarity interval (PF3r) that secures its correlation to

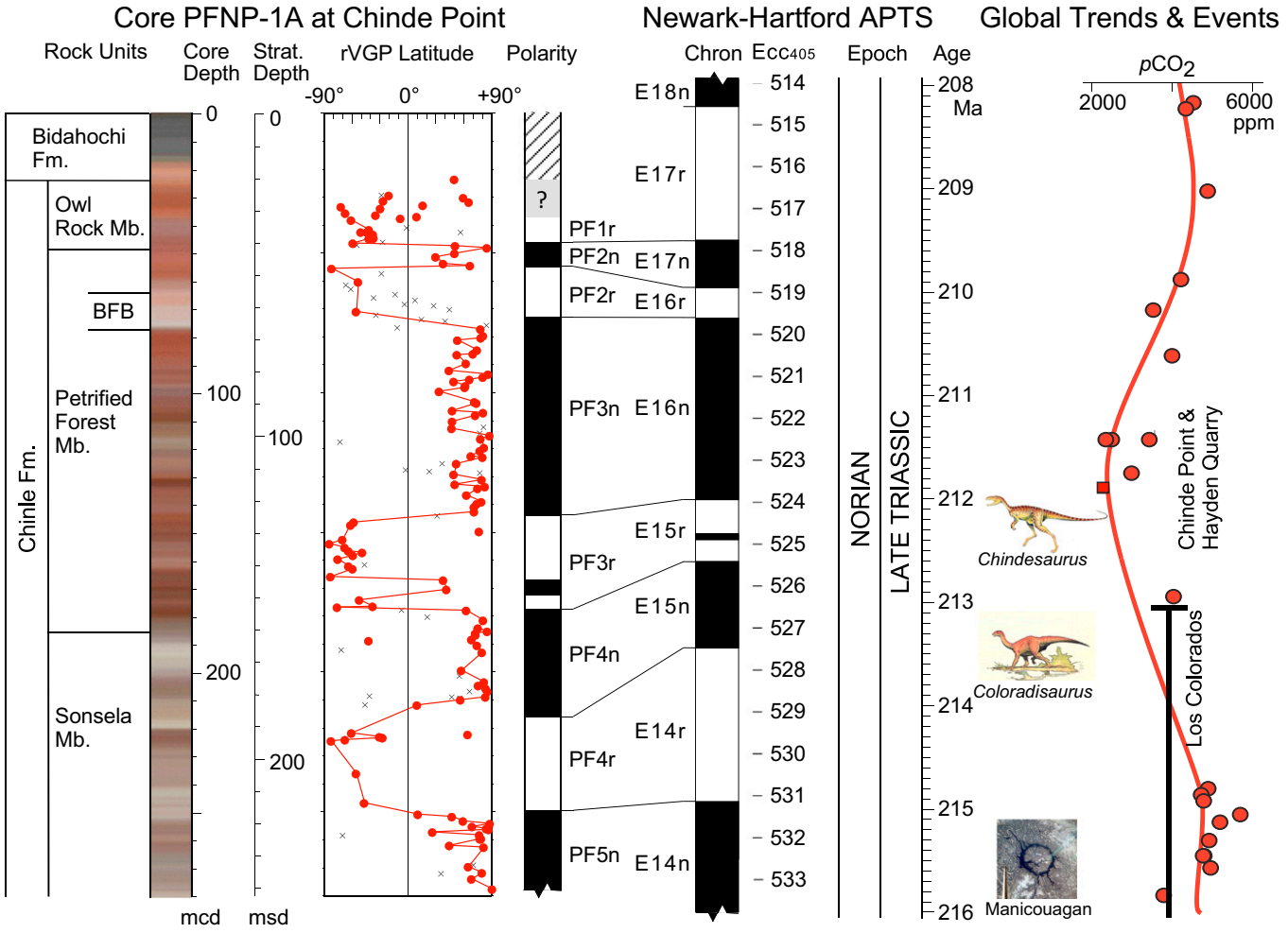

Fig. 2. Magnetostratigraphy of core PFNP-1A (for rock units and depth scale see legend to Fig. 1). rVGP latitudes are for sample ChRM directions converted to virtual geomagnetic poles whose rotated latitude with respect to the 210-Ma mean reference pole for North America (17) are plotted versus core (mcd) and stratigraphic (msd) depth for the upper Chinle Fm. Positive (northerly) and negative (southerly) rVGP latitudes correspond to normal and reverse polarity, delineated in polarity column by filled and open bars, respectively. Solid circles are accepted sample data with MAD values of 16° or less; crosses are rejected sample data (*SI Appendix*, Table S3). Proposed correlation indicates that the sampled section extends from around 209–215 Ma of the Newark–Hartford APTS chronology (1), which is based on a U–Pb-dated anchor at 201.6 Ma for 405-ky eccentricity cycles (k, peaks numbered from most recent at 0.216 Ma as k = 1 for Ecc_{405}:k). Some global events and trends in the Late Triassic that can be integrated with the age-validated APTS include the large-bodied sauropodomorph-rich La Esquina assemblage [e.g., *Coloradisaurus* (34)] in the upper part of the Los Colorados Fm. in the Ischigualasto Basin in Argentina (25), and the Revueltian assemblage of the Chinle Fm. with rare small-bodied theropod dinosaurs [e.g., *Chindesaurus* from the Petrified Forest Mb. in the PFNP, Arizona, and the Hayden Quarry at Ghost Ranch, New Mexico (24)] that is only about a million years younger and completely lacks sauropodomorphs. The 65-km-diameter Manicouagan impact crater in Quebec, Canada, has melt rocks dated by U–Pb zircon geochronology to 215.5 Ma (35) that are characterized by normal polarity (36). The atmospheric carbon dioxide concentration, pCO_2 in parts per million (ppm) is also shown as a red curve with data points as circles based on the paleosol proxy (37).

Chron E15r is well represented in the outcrop section. Paleomagnetic results were not obtained higher in the outcrop section that might have allowed identification of the critical PF2r magnetozone that straddles the BFB. Detrital zircons in an early study yielded U–Pb dates that indicated a likely, yet poorly defined, depositional age of 209 ± 5 Ma for the BFB (13). In a subsequent study, 16 prismatic zircons from a sample about 1.5 m above the base of the BFB at Chinde Point were analyzed by chemical abrasion–thermal ionization mass spectrometry (CA-TIMS); five distinguishably younger zircons gave a weighted mean U–Pb date of 209.93 ± 0.07 Ma (2σ) (12).

Here, we report a U–Pb CA-TIMS detrital zircon age of 210.08 ± 0.22 Ma for a coherent cluster of 6 out of 14 zircons analyzed from the BFB in core PFNP-1A (*SI Appendix*). The two U–Pb CA-TIMS zircon dates for the BFB differ by an insignificant 0.15 My. Sample 52Q2 (210.08 ± 0.22 Ma) in the BFB is from within magnetozone PF2r, which is correlated to Chron E16r whose APTS age range of 209.95–210.25 Ma was based on counting 20.62–21.35 long eccentricity (405 ky) cycles back from the high-precision U–Pb zircon date at 201.6 Ma in the Newark section (1, 7). The U–Pb CA-TIMS zircon date for the BFB agrees precisely with the predicted APTS age for Chron E16r. This agreement immediately discounts assertions that even a small fraction of a 405-ky cycle let alone millions of years are missing below the CAMP lavas in the Newark section.

The overall stratigraphic coherence of the magnetic correlations with the BFB and other U–Pb zircon dates can be gauged in a plot of depth versus age (Fig. 3). The magnetic correlations to the APTS (coefficient of determination, $R^2 = 0.9845$) suggest a relatively uniform net sediment accumulation rate of about 34.8 msd/My from the upper Sonsela, through the Petrified Forest, and up into the lower Owl Rock members. A tight linear regression of composite heights of lithostratigraphic members from outcrop (12, 20) versus their stratigraphic depths in PFNP-1A (*SI Appendix*,

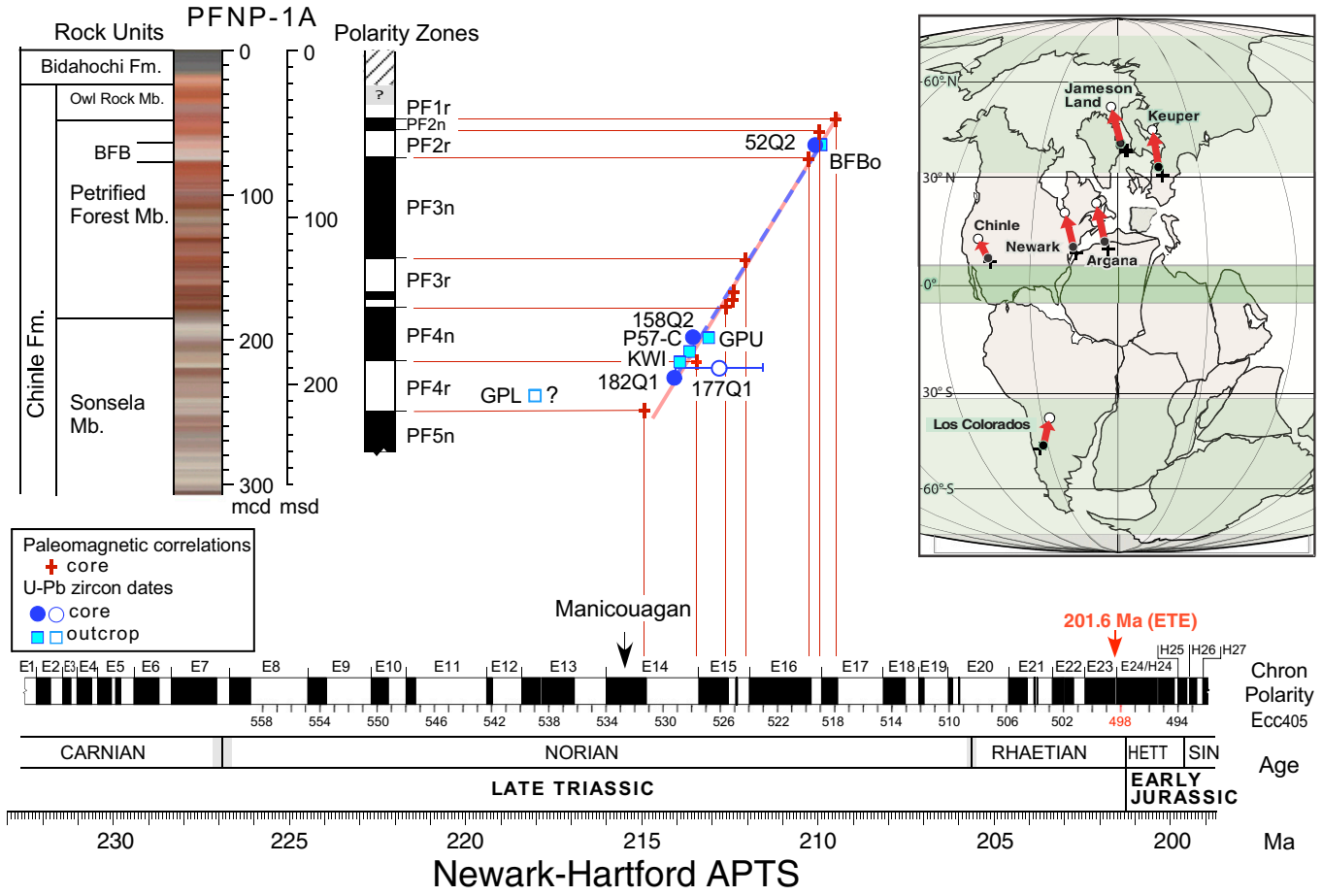

Fig. 3. Depth versus age plot for core PFNP-1A based on correlation of magnetostratigraphy with the Newark–Hartford APTS (1). Stratigraphic units, graduated depths, and color log of PFNP-1A core as in Figs. 1 and 2. Red crosses are magnetozone boundaries in PFNP-1A correlated to the APTS (*SI Appendix*, Table S2); solid red line is a linear regression for base magnetozone PF1r to base magnetozone PF4r to their correlative chron ages. Blue circles are U–Pb CA-TIMS detrital zircon dates from PFNP-1A reported here (*SI Appendix*, Table S4); light blue squares are published U–Pb CA-TIMS detrital zircon dates from outcrop correlated here to PFNP-1A using a regression on member boundaries mapped in an outcrop composite section (12, 20) versus those in PFNP-1A (*SI Appendix*, Fig. S5). Linear regression on U–Pb CA-TIMS dates (blue line) based on sample data from core PFNP-1A (excluding sample 177Q1), and by filled circles (see *SI Appendix*, Fig. S6 for regressions including U–Pb CA-TIMS zircon dates on outcrop samples). U–Pb zircon date for Manicouagan crater impact melt rocks (35), which are characterized by normal polarity (36), is shown for reference. *Inset* Shows a paleocontinental reconstruction of Pangea positioned according to a 220-Ma mean global paleopole (17) with some key continental localities indicated by filled circles connected by arrows to their relative positions at 200 Ma by open circles. Map adapted with permission from ref. 25.

Fig. S5 and Table S1) allows the U–Pb-dated levels in outcrop to be compared with those reported here from core PFNP-1A. The dates for the BFB from outcrop (sample BFBo) and core (sample 52Q2) are indistinguishable, as described above, supporting the use of the base of the distinctive BFB as a regional time horizon. Sample 158Q2 along with samples GPU and P57-C confirm that the included magnetozone PF4n indeed correlates to Chron E15n, whereas sample 182Q1 along with sample GPU confirm that included magnetozone PF4r most probably correlates to Chron E14r. However, sample GPL has a reported U–Pb CA-TIMS zircon date of 218.02 ± 0.28 Ma (12) that is much too old for its projected level at 207.8 msd in PFNP-1A, which would place it within magnetozone PF4r whose correlative Chron E14r ranges back to only 214.92 Ma (Fig. 3). Further discussion of GPL and other dated samples from outcrop lower in the Chinle Fm. are deferred pending acquisition of additional U–Pb CA-TIMS zircon dates directly from the core.

The U–Pb CA-TIMS zircon dates for samples 52Q2, 158Q2, and 182Q1 from the core are highly consistent with the depth–age relationship for samples BFBo, GPU, KWI, and P57-C from outcrop projected to PFNP-1A as described above (*SI Appendix*, Fig. S6). However, given the added stratigraphic uncertainties of projecting the dates from surface exposures to PFNP-1A, we prefer to use the dates obtained from the core (samples 52Q2, 158Q2, and 182Q1) for a more detailed analysis. This set of sample data provides a regression for Y (meters stratigraphic depth in PFNP-1A) with respect to X (age in Ma) (Y = 34.34 * X − 7,158; R^2 = 0.9994) that is in remarkably close agreement with a regression of predicted depth versus ages from the APTS via magnetostratigraphy (Y = 34.84 * X − 7,258 m; R^2 = 0.9845) and yield highly consistent estimates for sediment accumulation rate of 34.3–34.8 m/My (Fig. 3).

Discussion

The very close agreement between the ages predicted by the magnetic polarity correlations and the U–Pb zircon geochronology directly confirms the timing of the APTS back to about 215 Ma, at around the Chron E14r/14n boundary; this immediately refutes suggestions that significant time is missing in the Newark–Hartford sequence used to build the APTS. The congruence between the Colorado Plateau–zircon-calibrated polarity timescale and the Newark–Hartford APTS can be directly attributed to the reliability of the 405-ky eccentricity variation recorded in the Newark–Hartford sequence, in terms of its correct identification and

counting of its expression as the long eccentricity climate cycle (21) as well as the periodicity being close to 405 ky as calculated from modern celestial mechanics (6). In fact, the age difference (8.50 My) estimated from slightly less than 21 long eccentricity cycles between the U–Pb-dated tie points at 210.08 Ma for the BFB within Chron E16r (Ecc_{405}:518.87–519.60, centered at 519.24), and 201.6 Ma just below first CAMP basalt (Ecc_{405}:498.25) is indistinguishable from the difference in the U–Pb dates (8.48 My, with an estimated uncertainty of ±0.3 My from propagation of the individual 2σ errors), which would imply a cycle duration of close to 404 ky, or within an insignificant 1 ky or 0.25% of the hypothesized 405-ky period. The periodicity of the Jupiter–Venus-long eccentricity cycle indeed must be very close to 405 ky even at this remote age range and we see no justification given the present observational uncertainties to assume a different value.

The 405-ky oscillation is the largest and most stable term in the periodic approximation of Earth's eccentricity, but theoretical solutions formally constrain orbital motions to only about the past 50 million years, with different solutions yielding deviations of up to about ±405 ky over 250 My (6). Nonetheless, this apparent stability, however plausible, is entirely theoretical. Independent U–Pb CA-TIMS zircon dating is just beginning to confirm the accuracy of these solutions in the Cenozoic (22). Our work shows that the 405-ky eccentricity cycle can be used with confidence as a framework of geologic timescales back to at least 215 Ma in the Late Triassic, which also places an empirical constraint on the dynamics of the Solar System (6) over a time span more than four times longer than orbital solutions allow.

Finally, a number of global events in the Late Triassic can now be integrated more confidently into the framework of the APTS (Fig. 2). In particular, the vexing problem of Late Triassic biotic provinciality and the delay in rise to ecological dominance of tropical dinosaurs until after the end-Triassic mass extinction (23) can be explored without relying on biostratigraphy for time control, which has in the past resulted in circular reasoning. Dinosaurs had evolved by the early Late Triassic (Carnian), and by the Norian, relatively large, herbivorous, sauropodomorph dinosaurs were abundant at mid-to-high latitudes, but apparently absent from low latitudes (23, 24). Based on correlation of paleomagnetic polarity sequences to the confirmed APTS, we can now more securely place the diverse La Esquina assemblage, with its abundant large herbivorous sauropodomorph dinosaurs from the upper third of the Los Colorados Formation of Argentina (paleolatitude ~40° S; Fig. 3, *Inset*) in Chron E15n at about 213 Ma (25). This assemblage is thus contemporaneous with the diverse assemblages of the early part of the Revueltian biozone (18) of the western United States (paleolatitude, ~10°N), in which dinosaurs are rare and small-bodied, and sauropodomorphs (and all herbivorous dinosaurs) are absent (26). Like in the western United States, strata in chrons E15n-E16n in the Newark and Fundy basins (27) with paleolatitudes of ~15°N produce diverse tetrapod track assemblages but lack putative sauropodomorph footprints, and dinosaur track-makers are rare and small-bodied. The Fleming Fjord Fm. bone and track assemblages from Greenland (paleolatitude, ~43°N) have both abundant large-bodied sauropodomorph skeletons and footprints (28) and correlate to chrons possibly only as old as E14n (~216 Ma) (29), similar in age to the La Esquina assemblage in the Los Colorados Fm. as well to the Revueltian assemblages in the Chinle and contemporaneous assemblages in the Newark and Fundy basins. The absence of large-bodied herbivorous dinosaurs in the tropics of Pangea, the strong biotic provinciality (30, 31), and the 30-My delay in the rise of dinosaurian ecological dominance in the tropics (23), is thus not an artifact of biostratigraphic miscorrelation as construed by some (32) but a real feature of that world in which it can now be quantified both in time and space.

Materials and Methods

A total of 174 oriented subsamples were extracted from ~24–278 mcd (~21–248 msd) from the finest-grained most red-colored sediment facies of the lower Owl Rock Mb., the entire Petrified Forest Mb. including the BFB, and down into the middle part of the Sonsela Mb. Progressive thermal demagnetization was used to isolate the characteristic component of the natural remanent magnetization of each specimen that tended to be carried predominantly by hematite (*SI Appendix*, Fig. S1). A least-squares linear fit using principal-component analysis over the three to seven (typically five) demagnetization steps in the range of 300–600 °C and anchored to the origin (*SI Appendix*, Fig. S2) was used to assess the characteristic remanent magnetization (ChRM) in each sample. Results were deemed acceptable if the maximum angular deviation (MAD) (33) was 16° or less; 132 of the 174 samples (76%) satisfied this criterion (average MAD of 8°) and fell into two populations (*SI Appendix*, Fig. S3), shallow northerly and shallow southerly groupings that are interpreted to represent normal and reverse polarities of the Late Triassic geomagnetic field that provide a magnetostratigraphy (*SI Appendix*, Tables S2 and S3).

Samples for U–Pb zircon dating were also taken at the Rutgers Core Repository. Each sample was a 10- to 20-cm-thick quarter-round cut using a bandsaw with a carborundum-tipped blade, targeting sandstones that were poorly sorted and contain abundant accessory minerals indicative of volcanic detritus. The samples were crushed, and mineral concentrates were then purified using standard mineral separation techniques, including sieves, magnetic separation, and density separation at the LaserChron Center at the University of Arizona, mounted on epoxy disks and polished to about one-half of the crystal width followed by laser ablation-inductively coupled plasma mass spectrometry (LA-ICPMS) analyses, providing a survey of the range of zircon ages present. At the Berkeley Geochronology Center, 20–30 crystals displaying the youngest LA-ICPMS age from each sample were extracted from the mount and prepared for zircon U–Pb chemical abrasion, thermal ionization mass spectroscopy (CA-TIMS). Before TIMS analysis, all zircons were pretreated using thermal annealing at 850 °C for 48 h, followed by chemical abrasion with concentrated HF in pressurized dissolution capsules at 220 °C for 8–12 h. The analytical data of four samples from the Chinle Fm. subjected to U–Pb zircon CA-TIMS analyses are presented in *SI Appendix*, Fig. S4 and Tables S4 and S5.

ACKNOWLEDGMENTS. We thank the National Park Service, particularly superintendent Brad Traver, for permission to core in the park and for logistical support during site selection and drilling. On-site and laboratory core processing, scanning, and archiving were carried out by LacCore, particularly Anders Noren, Kristina Brady, and Ryan O'Grady; on-site core-handling volunteers Justin Clifton, Bob Graves, Ed Lamb, Max Schnurrenberger, and Brian Switek are thanked for their around-the-clock efforts, and drilling manager Doug Schnurrenberger for overseeing a superb coring project. We sincerely thank the two journal reviewers for insightful comments that allowed us to improve the data analyses. This project was funded by National Science Foundation (NSF) Collaborative Grants EAR 0958976 (to P.E.O. and J.W.G.), 0958723 (to R.M.), 0958915 (to R.B.I.), 0959107 (to G.E.G.), and 0958859 (to D.V.K.), and by Deutsche Forschungsgemeinschaft for International Continental Scientific Drilling Program support. Additional support was provided by NSF Grant EAR-1338583 (to G.E.G.) to the Arizona LaserChron Center; P.E.O. acknowledges support from the Lamont-Climate Center, R.M. acknowledges support of the Ann and Gordon Getty Foundation, and D.V.K. is grateful to the Lamont–Doherty Incentive Account for support of the Paleomagnetics Laboratory. Curatorial facilities for the work halves of the CPCP cores are provided by the Rutgers Core Repository. Any opinions, findings, or conclusions of this study represent the views of the authors and not those of the US Federal Government. This is a contribution to IGCP-632, and is Petrified Forest Paleontological Contribution 54, and Lamont–Doherty Earth Observatory Contribution 8208.

1. Kent DV, Olsen PE, Muttoni G (2017) Astrochronostratigraphic polarity time scale (APTS) for the Late Triassic and Early Jurassic from continental sediments and correlation with standard marine stages. *Earth Sci Rev* 166:153–180.
2. Kent DV, Olsen PE, Witte WK (1995) Late Triassic-earliest Jurassic geomagnetic polarity sequence and paleolatitudes from drill cores in the Newark rift basin, eastern North America. *J Geophys Res* 100:14965–14998.
3. Olsen PE, Kent DV, Cornet B, Witte WK, Schlische RW (1996) High-resolution stratigraphy of the Newark rift basin (early Mesozoic, eastern North America). *Geol Soc Am Bull* 108:40–77.
4. Olsen PE, Kent DV (1996) Milankovitch climate forcing in the tropics of Pangea during the Late Triassic. *Palaeogeogr Palaeoclimatol Palaeoecol* 122:1–26.
5. Kent DV, Olsen PE (2008) Early Jurassic magnetostratigraphy and paleolatitudes from the Hartford continental rift basin (eastern North America): Testing for polarity bias and abrupt polar wander in association with the Central Atlantic Magmatic Province. *J Geophys Res* 113:B06105.
6. Laskar J, Fienga A, Gastineau M, Manche H (2011) La2010: A new orbital solution for the long-term motion of the Earth. *Astron Astrophys* 532:81–15.
7. Blackburn TJ, et al. (2013) Zircon U–Pb geochronology links the end-Triassic extinction with the Central Atlantic Magmatic Province. *Science* 340:941–945.

8. Muttoni G, et al. (2004) Tethyan magnetostratigraphy from Pizzo Mondello (Sicily) and correlation to the Late Triassic Newark astrochronological polarity time scale. *Geol Soc Am Bull* 116:1043–1058.
9. Olsen PE, Reid JC, Taylor K, Whiteside JH, Kent DV (2015) Revised stratigraphy of Late Triassic age strata of the Dan River Basin (Virginia and North Carolina, USA) based on drill core and outcrop data. *Southeast Geol* 51:1–31.
10. Van Veen PM (1995) Time calibration of Triassic/Jurassic microfloral turnover, eastern North America—comment. *Tectonophysics* 245:91–95.
11. Tanner LH, Lucas SG (2015) The Triassic–Jurassic strata of the Newark basin, USA: A complete and accurate astronomically-tuned timescale? *Stratigraphy* 12:47–65.
12. Ramezani J, et al. (2011) High-precision U–Pb zircon geochronology of the Late Triassic Chinle Formation, Petrified Forest National Park (Arizona, USA): Temporal constraints on the early evolution of dinosaurs. *Geol Soc Am Bull* 123:2142–2159.
13. Riggs MR, Ash SR, Barth AP, Gehrels GE, Wooden JL (2003) Isotopic age of the Black Forest Bed, Petrified Forest Member, Chinle Formation, Arizona: An example of dating a continental sandstone. *Geol Soc Am Bull* 115:1315–1323.
14. Steiner MB, Lucas SG (2000) Paleomagnetism of the Late Triassic Petrified Forest Formation, Chinle Group, western United States: Further evidence of "large" rotation of the Colorado Plateau. *J Geophys Res* 105:25791–25808.
15. Zeigler KE, Parker WG, Martz JW (2017) The Lower Chinle Formation Late Triassic at Petrified Forest National Park, Southwestern USA: A case study in magnetostratigraphic correlations. *Terrestrial Depositional Systems Deciphering Complexities through Multiple Stratigraphic Methods*, eds Zeigler KE, Parker WG (Elsevier, Amsterdam), pp 251–293.
16. Olsen PE, et al. (2010) The Colorado Plateau Coring Project (CPCP): 100 million years of Earth system history. *Earth Science Frontiers* 17:55–63.
17. Kent DV, Irving E (2010) Influence of inclination error in sedimentary rocks on the Triassic and Jurassic apparent polar wander path for North America and implications for Cordilleran tectonics. *J Geophys Res* 115:B10103.
18. Martz JW, Parker WG (2017) Revised formulation of the Late Triassic land vertebrate "Faunachrons" of western North America: Recommendations for codifying nascent systems of vertebrate b. *Terrestrial Depositional Systems*, eds Zeigler KE, Parker WG (Elsevier, Amsterdam), pp 39–124.
19. Lepre CJ (2017) Crevasse-splay and associated depositional environments of the hominin-bearing lower Okote Member, Koobi Fora Formation (Plio-Pleistocene), Kenya. *The Depositional Record* 3:161–186.
20. Atchley SC, et al. (2013) A linkage among Pangean tectonism, cyclic alluviation, climate change, and biologic turnover in the Late Triassic: The record from the Chinle Formation, southwestern United States. *J Sediment Res* 83:1147–1161.
21. Olsen PE, Kent DV (1999) Long-period Milankovitch cycles from the Late Triassic and Early Jurassic of eastern North America and their implications for the calibration of the Early Mesozoic time-scale and the long-term behaviour of the planets. *Philos Trans R Soc Lond A* 357:1761–1786.
22. Sahy D, Condon DJ, Terry DO, Fischer AU, Kuiper KF (2015) Synchronizing terrestrial and marine records of environmental change across the Eocene–Oligocene transition. *Earth Planet Sci Lett* 427:171–182.
23. Whiteside JH, et al. (2015) Extreme ecosystem instability suppressed tropical dinosaur dominance for 30 million years. *Proc Natl Acad Sci USA* 112:7909–7913.
24. Irmis RB, Mundil R, Martz JW, Parker WG (2011) High-resolution U–Pb ages from the Upper Triassic Chinle Formation (New Mexico, USA) support a diachronous rise of dinosaurs. *Earth Planet Sci Lett* 309:258–267.
25. Kent DV, Santi Malnis P, Colombi CE, Alcober OA, Martínez RN (2014) Age constraints on the dispersal of dinosaurs in the Late Triassic from magnetochronology of the Los Colorados Formation (Argentina). *Proc Natl Acad Sci USA* 111:7958–7963.
26. Nesbitt SJ, Irmis RB, Parker WG (2007) A critical reevaluation of the Late Triassic dinosaur taxa of North America. *J Syst Palaeontology* 5:209–243.
27. Kent DV, Olsen PE (2000) Magnetic polarity stratigraphy and paleolatitude of the Triassic-Jurassic Blomidon Formation in the Fundy basin (Canada): Implications for early Mesozoic tropical climate gradients. *Earth Planet Sci Lett* 179:311–324.
28. Clemmensen LB, et al. (2016) The vertebrate-bearing Late Triassic Fleming Fjord Formation of central East Greenland revisited: Stratigraphy, palaeoclimate and new palaeontological data. *Geol Soc Lond Spec Publ* 434:31–47.
29. Kent DV, Clemmensen LB (1996) Paleomagnetism and cycle stratigraphy of the Triassic Fleming Fjord and Gipsdalen formations of East Greenland. *Bull Geol Soc Den* 42: 121–136.
30. Olsen PE, Galton PM (1984) A review of the reptile and amphibian assemblages from the Stormberg of southern Africa, with special emphasis on the footprints and age of the Stormberg. *Palaeontologia Africana* 25:87–110.
31. Whiteside JH, Grogan DS, Olsen PE, Kent DV (2011) Climatically driven biogeographic provinces of Late Triassic tropical Pangea. *Proc Natl Acad Sci USA* 108:8972–8977.
32. Lucas SG (2018) Late Triassic terrestrial tetrapods: Biostratigraphy, biochronology and biotic events. *The Late Triassic World: Earth in a Time of Transition*, Topics in Geobiology, ed Tanner LH (Springer, New York), Vol 46, pp 351–405.
33. Kirschvink JL (1980) The least-squares line and plane and the analysis of palaeomagnetic data. *Geophys J R Astron Soc* 62:699–718.
34. Apaldetti C, Martinez RN, Pol D, Souter T (2014) Redescription of the skull of *Coloradisaurus brevis* (Dinosauria, Sauropodomorpha) from the Late Triassic Los Colorados Formation of the Ischigualasto-Villa Union Basin, northwestern Argentina. *J Vertebr Paleontol* 34:1113–1132.
35. Ramezani J, Bowring SA, Pringle MS, Winslow FD, Rasbury ET (2005) The Manicouagan impact melt rock: A proposed standard for the intercalibration of U–Pb and $^{40}Ar/^{39}Ar$ isotopic systems. *Geochim Cosmochim Acta* 69:A321.
36. Eitel M, Gilder SA, Spray J, Thompson L, Pohl J (2016) A paleomagnetic and rock magnetic study of the Manicouagan impact structure: Implications for crater formation and geodynamo effects. *J Geophys Res* 121:436–454.
37. Schaller MF, Wright JD, Kent DV (2015) A 30 million-year record of Late Triassic pCO_2 variation supports a fundamental control of the carbon-cycle by changes in continental weathering. *Geol Soc Am Bull* 127:661–671.
38. Martz JW, Parker WG (2010) Revised lithostratigraphy of the Sonsela Member (Chinle Formation, Upper Triassic) in the southern part of Petrified Forest National Park, Arizona. *PLoS One* 5:e9329.

PNAS
www.pnas.org

Supplementary Information for

Empirical evidence for stability of the 405 kyr Jupiter-Venus eccentricity cycle over hundreds of millions of years

Dennis V. Kent[1,2]
Paul E. Olsen[2]
Cornelia Rasmussen[3]
Christopher Lepre[1,2]
Roland Mundil[4]
Randall B. Irmis[3,5]
George E. Gehrels[6]
Dominique Giesler[6]
John W. Geissman[7]
William G. Parker[8]

[1]Earth & Planetary Sciences, Rutgers University, Piscataway, NJ 08854
[2]Lamont-Doherty Earth Observatory of Columbia University, Palisades, NY 10964
[3]Department of Geology & Geophysics, University of Utah, Salt Lake City, UT 84112
[4]Berkeley Geochronology Center, 2455 Ridge Rd., Berkeley CA 94709
[5]Natural History Museum of Utah, University of Utah, Salt Lake City, UT 84108
[6]Department of Geosciences, University of Arizona, Tucson, AZ 85721
[7]Department of Geosciences, University of Texas at Dallas, Richardson, TX 75080
[8]Petrified Forest National Park, Petrified Forest, AZ 86028

Corresponding author: Dennis Kent
Email: dvk@rutgers.edu

This PDF file includes:

Supplementary text
Figs. S1 to S7
Tables S1 to S5
References for SI reference citations

Supplementary Text

PFNP-1A core logistics and sampling

Core CPCP-PFNP-13-1A (henceforth PFNP-1A) was drilled in the parking lot at Chinde Point in the northern part of the Petrified Forest National Park (35.085933° N, 109.795500° W, WGS84 datum) in November and December, 2013, by Ruen Drilling, Inc. The HQ core hole configuration was designed to be inclined 60° from horizontal (to facilitate orientation of cores in the flat-lying beds) at an azimuth of 135° (to avoid a late Cenozoic Bidahochi lava feeder dike). EZ Shot data collected during drilling give core hole inclinations ranging from 58.3° - 62.0° and azimuths (true north) from 132.2° - 140.3°, conforming to the design specifications. Accordingly, we use an inclination of 60° and azimuth of 135° to reorient samples taken from the core. The drilled interval had a total core length of 519.9 m (450.0 m stratigraphic equivalent assuming the hole was inclined at 60° and beds are horizontal). The 6.25-cm-diameter core was collected in 395 runs, each nominally 1.5 m long. Each run was cut into two to three segments (each not exceeding 76.2 cm for scanning purposes) for a total of 931 sections. Orientation of each core run was performed using the Reflex ACT II(III) device. A video of how this device works and how the data are transferred to the core is at: http://www.youtube.com/user/reflexinstruments, with the relevant video being: https://www.youtube.com/watch?v=FrPKM-_D72A.

The core orientation information was transferred from the device to the bottom of each core. Core in its liner was transferred to the onsite LacCore tent where a white line was drawn from the orientation mark along the core axis length before being sliced into core segments. The white line is consistent for all cores, and always on the down-side of the core opposite from the azimuth of the inclined drilled hole. The up/down orientation of the core segments is maintained with blue endcaps on tops and red endcaps on bottoms of liners. In a small proportion of cases the orientation is ambiguous or reversed due to a bad orientation device reading (one of the two devices was not working for a period of time), the core rotating inside the plastic liner, or possibly due to operator error during core cutting and labeling in the lab. At LacCore, the core segments were split along the white line up with a 12” diameter diamond saw lubricated with water. After scanning and description, the work-halves of the cores were shipped to the Rutgers Core Repository. Looking down the borehole, the work halves of the cores would be on the observer’s left side, i.e., the northeast half of the core with the split face toward the southwest.

Sediments above the Sonsela Mb. in the core were generally too poorly indurated to take standard 2.5 cm-diameter plugs with a water-cooled diamond drill bit. An initial suite of samples was thus taken mostly by plucking loose pieces from the split face of the working-halves of the cores. The subsequent and preferred method of sampling to obtain coherent material was to cut half-round or quarter-round slices about 2 cm thick, sometimes through the plastic liner, using a bandsaw with a carborundum-tipped blade. Specimens for paleomagnetic measurements were prepared by cutting a flat surface on the up-core side and a perpendicular flat surface parallel to the split-face of the core. The split-face sample surface was inscribed with an arrow marking the up-core direction on what should be an oriented face as determined from the Reflex device. Fine-grained reddish-colored sediment was preferentially sampled although this lithology was often associated with massive paleosols that had few indictors of bedding; silt- and sand-sized sediment with layering and oblate bleached haloes around organic blebs or minerals (with major axes assumed parallel to bedding) were sometimes present in the same core run and such indicators of

bedding provided an independent check on the orienting tool. Given the known azimuth and dip of the drill core, traces of bedding that are horizontal *in situ* should appear to tilt 30° down to the right looking at the split face of the working-halves of the core, for the interval studied here.

Background information on core PFNP-1A can be found at http://www.ldeo.columbia.edu/~polsen/cpcp/CPCP_Scientific_Drilling.html.

Paleomagnetic analyses

Backfield demagnetization curves of isothermal remanent magnetization (IRM) show that the magnetizations of the sampled units are typically dominated by hematite, as indicated by lack of saturation in 2.5 T fields and high remanent coercivities of about 700 mT, with some contributions of a lower coercivity phase like magnetite that even become dominant in some of the pale-colored sandstones of the BFB (**Fig. S1**). Accordingly, progressive thermal demagnetization was used to isolate the characteristic component of the natural remanent magnetization (NRM) of each specimen. Samples were heated at temperature for 45 minutes in a ASC TD48 oven in typically 12 steps from 100° (or 150°) to 675°C and the magnetizations after each step were measured after cooling to room temperature in a 2G Model 760 3-axis DC SQUID magnetometer, all housed in a magnetically-shielded room at LDEO.

Vector endpoint demagnetograms (**Fig. S2**) typically show the removal of a spurious (not systematically oriented) low unblocking temperature component to 300°C followed in most samples by a stable component with shallow inclination up to 675°C. A least-squares linear fit using principal component analysis over the 3 to 7 (typically 5) demagnetization steps in the range 300°–600°C and anchored to the origin was used to assess the characteristic remanent magnetization (ChRM) in each sample. The 132 sample characteristic remanent magnetizations (ChRM) that were deemed acceptable based on progressive thermal demagnetization (maximum angular deviation (MAD) (1)) of 16° or less (average MAD 8°) are quite scattered but generally fall into two populations (**Fig. S3**), a northerly-directed group (Dec=0.4°, Inc=+22.7°, a95=6.0°, k=7.1, n=90) and a southerly-directed group (Dec=172.8°, Inc=+8.1°, a95=12.5°, k=4.1, n=42). The declinations are close to 180° apart but there is a downward bias in the inclinations so the two populations are not antipodal (departure=32±14°) and do not pass a reversal test (2). The overall mean direction after inverting the southerly population is Dec=358.1°, Inc=+13.8°, a95=6.1°, k=5.0 for n=132 samples. The ChRM of approximately equivalent strata in outcrop had essentially the same mean direction (Dec=358.9° Inc=+8.2°) although with considerably less scatter (a95=2.8°, k=33.8 for n=53 samples from Painted Desert Mb., equivalent to Petrified Forest Mb. here) and passed a reversal test (Table 1 in (3)). The expected direction for the core site locality using the 210 Ma reference pole for North America (64.2°N 91.2°E A95=2.9°)(4) is Dec=350.9° Inc=20.6°, corresponding to a paleolatitude of 10.7°N±2.9°. The shallower than expected mean ChRM direction of the upper Chinle in core PFNP-1A (and in outcrop (3)) can be attributed to sedimentary inclination error corresponding to a flattening factor of ~0.7, typical of many Triassic continental redbeds with early-acquired magnetizations (5). The accepted sample data were used to construct a paleomagnetic polarity sequence for the upper 280 mcd of core PFNP-1A (**Tables S2, S3**).

U-Pb CA-TIMS analytical procedures

The samples were crushed and mineral concentrates were then purified using standard mineral separation techniques, including sieves, magnetic separation and density separation at the

LaserChron Center at University of Arizona, mounted on epoxy disks and polished to about one-half of the crystal width followed by LA-ICPMS analyses providing a survey of the range of zircon ages present. At the Berkeley Geochronology Center (BGC) 20-30 crystals displaying the youngest LA-ICPMS age from each sample were extracted from the mount and prepared for zircon U-Pb CA-TIMS (Chemical Abrasion-Thermal Ionization Mass Spectrometry). Prior to TIMS analysis all zircons were pretreated using thermal annealing at 850°C for 48 hrs, followed by chemical abrasion with concentrated HF in pressurized dissolution capsules at 220°C for 8 to 12 hrs. Complete dissolution in an ultraclean wet chemistry laboratory was preceded by cleaning the crystals in ultrasonically agitated aqua regia followed by multiple steps of rinsing in clean HNO_3. Zircon crystals were then spiked with ^{205}Pb-^{233}U- ^{235}U tracer solution (both a solution mixed and calibrated at BGC as well as Earthtime 535 tracer were used; for intercalibration see Ref. (6)), and then dissolved by vapor transfer in HF using miniature PTFE capsules at 220°C for 6 days. After dissolution, the equilibrated sample/tracer solution was loaded on zone refined Re filament using silica gel as emitter substance (7). Isotope ratios were determined on a Micromass Sector 54 mass spectrometer using a Daly-type ion counter positioned behind a WARP filter. Pb (as Pb^+) and U (as UO^{2+}) were run sequentially on the same filament (for calibration of the BGC tracer see (6, 8, 9)). Repeat measurements of the total procedural blank averaged 0.82 ± 0.36 pg Pb (U blanks were indistinguishable from zero), with $^{206}Pb/^{204}Pb$ = 18.40 ± 0.46, $^{207}Pb/^{204}Pb$ = 15.64 ± 0.25, $^{208}Pb/^{204}Pb$ = 38.04 ± 0.75 (all 2σ of population), and a $^{206}Pb/^{204}Pb$-$^{207}Pb/^{204}$ Pb correlation of +0.47 (ratios and uncertainties were propagated into the age and age-error calculations). The total procedural blank including ion exchange chemistry is also as low as 1 pg but scatter in total common Pb concentration and possibly common Pb composition suggests that results from unextracted analyses of zircon yield better reproducibility. Deficient radiogenic ^{206}Pb in zircon due to initial deficit of ^{230}Th is accounted for by assuming a partition coefficient ratio DTh/DU of 0.2 (as applied in (10)), or by assuming Th/U in the parent magma to be 3.5 where the ET535 tracer solution was used (the resulting difference in age from either approach is negligible). Mass fractionation of U during analysis was controlled by the U double spike, whereas Pb mass fractionation was corrected by 0.15 ± 0.6 %/AMU (based on multiple analyses of NBS 981).

U-Pb CA-TIMS results

The analytical data of four samples from the Chinle Fm subjected to U-Pb zircon CA-TIMS analyses (**Fig. S4**) are presented below. The ages are considered maximum depositional ages because the zircons contained in the deposits are redeposited and the lag between the ages of juvenile volcanic zircons and deposition is unknown but arguably short or not even resolvable. Therefore ages reported here, which serve to constrain the ages of corresponding polarity zones in the Late Triassic of the Colorado Plateau and the astronomically calibrated Newark Hartford basin, are not considered to represent accurate depositional ages by themselves.

Ages are reported as weighted mean $^{206}Pb/^{238}U$ ages (with uncertainties at the 95% confidence level) unless stated otherwise **(Tables S4, S5)**.

Sample 52Q-2 from 56.0 ± 0.08 msd is a fine-grained white sandstone from the Black Forest Bed within the upper part of the Petrified Forest Mb. in polarity zone PF2r. An age of 210.08 ± 0.22 Ma (MSWD = 0.82) can be calculated from a coherent cluster of 6 out 14 analyses. Seven older analyses range from 210.52 to 214.92 Ma, and one age is resolvably younger at 203.06 Ma

and likely compromised by Pb loss. Th/U in this sample ranges from 0.38 to 1.97, which suggests, due to the wide range, that the crystals are derived from various sources. Our age of 210.08 ± 0.22 Ma is in agreement with an age of 209.926 ±0.072 Ma reported for the Black Forest Bed, but not necessarily from exactly the same stratigraphic level. PF2r correlates with E16r with an astronomically tuned age range from 209.9 to 210.2 Ma.

Sample 158Q-2 is a sandstone from 172.0 ± 0.09 msd in the uppermost Sonsela Mb. and the middle portion of polarity zone PF4n. $^{206}Pb/^{238}U$ ages of 17 zircon analyzed range from 207.88 to 223.82 Ma, but ages <210 Ma are not feasible because of stratigraphic and age constraints from sample 52Q-2 9 (see below). We therefore conclude that at least the youngest 4 analyses of 158Q-2 suffered Pb loss despite an aggressive pretreatment of chemical abrasion. A cluster of nine analyses yields an age of 213.55 ± 0.28 Ma, however, the MSWD is elevated (2.0) suggesting that a subset of this cluster is representative of the maximum depositional age (either 213.00 ± 0.36 Ma or 213.71 ± 0.20 Ma if Pb loss is more severe). Th/U in the sample ranges from 0.70 to 1.66. Polarity zone PF4n correlates with E15n from the Newark Hartford basin with a predicted age from 212.6 to 213.4 Ma.

Sample 177Q-1 from 190.0 ± 0.09 msd is stratigraphically lower from the upper Sonsela Mb and also from within polarity zone PF4r. The $^{206}Pb/^{238}U$ ages are dispersed and range from 212.81 to 216.37 Ma with Th/U ranging from 0.64 to 1.85 (the latter can perhaps be considered an outlier). Some of the ages are also compromised by imprecision due to very small sample size. At face value the youngest age of 212.81 ± 1.25 Ma must be considered a maximum depositional age if Pb loss can be excluded. Because none of the ages were convincingly reproduced, the latter age is ambiguous.

Sample 182Q-1 from 195.3 ± 0.13 msd is a mud/siltstone from the upper Sonsela Mb. that was dated to an age of 214.08 ± 0.20 Ma (MSWD = 1.02) based on the youngest 6 analyses. Five additional analyses from selected crystals range from 214.88 to 219.54 Ma. Th/U of the crystals from the coherent cluster ranges from 0.49 to 1.05. Sample 182Q-1 is from within polarity zone PF4r which, based on the correlation with the APTS, is equivalent to polarity zone E14r (213.4 to 214.9 Ma).

Correlation of samples from core PFNP-1A and outcrop composite section

The BFB is a distinctive, white tuffaceous crossbedded sandstone that can be traced over large areas of the PFNP. Moreover, it was sampled for dating (11) in outcrop at Chinde Point, the same area as the drilling site for PFNP-1A, making its correlation to the core secure. In contrast, other dated horizons reported from the Sonsela Mb. (as well as the Blue Mesa and Mesa Redondo Members that are not considered here) of the Chinle Fm. (11-13) are from less distinctive beds sampled over a wide geographic area and thus present more of a challenge tying them into PFNP-1A. We use a lithostratigraphic composite section measured for the Chinle Fm. in outcrop (11, 12) as a framework for the U-Pb dates from outcrop samples. There is actually a remarkably good correlation between the cumulative thickness of lithostratigraphic subdivisions of the Chinle Fm. measured in outcrop and their stratigraphic thicknesses in core PFNP-1A, with a coefficient of determination, R^2>0.99 (**Fig. S5; Table S1**). We use the regression from the base of the Sonsela Mb. to the base of the Owl Rock Mb. pinned to the common base of the BFB to place the U-Pb CA-TIMS zircon data from outcrops analyzed by the MIT lab of the BFB and the Sonsela Mb. (11, 13) into the common lithostratigraphic depth scale for comparison with the U-Pb CA-TIMS

zircon data analyzed by the BGC lab and reported here from core PFNP-1A (**Table S4**). Depth relationships of the MIT outcrop samples and the BGC core sample data are very similar (**Fig. S6**). Given the added stratigraphic uncertainties of projecting the MIT outcrop dates to PFNP-1A, we prefer to use the BGC dates taken from the core (samples 52Q2, 158Q2 and 182Q1), which provide a linear regression (msd in core PFNP-1A = 34.34 * Age - 7158, R^2=0.999) that turns out to be remarkably close to a regression of predicted stratigraphic depth versus ages from the APTS via magnetostratigraphy (msd in core PFNP-1A = 34.84 * Age - 7258, R^2=0.985) (**Fig. 3**).

The high level of agreement between the APTS and U-Pb CA-TIMS dates, which shows that hiatuses are not apparent in the APTS, offers a unique opportunity to test the accuracy of the detrital zircon ages in terms of age bias due to redeposition. A linear fit with such high correlation of determination (R^2>0.99) to the CA-TIMS zircon ages suffices because, a priori, the magnitude of age bias due to redeposition is not known. However, some of this bias could be estimated from the departures of zircon ages from the APTS ages, if assumed to be accurate. For example, application of the StalAge algorithm with a Monte Carlo technique (14) to the verified APTS ages (**Fig. S7**) reveals small-scale offsets from a linear age-depth relationship that are most likely due to varying age biases in the populations of redeposited zircons. Such an approach might be useful to extract depositional ages from large populations of LA-ICPMS detrital zircon dates.

References

1. Kirschvink JL (1980) The least-squares line and plane and the analysis of palaeomagnetic data. *Geophysical Journal of the Royal Astronomical Society* 62:699-718.
2. McFadden PL & McElhinny MW (1990) Classification of the reversal test in palaeomagnetism. *Geophysical Journal International* 103:725-729.
3. Steiner MB & Lucas SG (2000) Paleomagnetism of the Late Triassic Petrified Forest Formation, Chinle Group, western United States: Further evidence of "large" rotation of the Colorado Plateau. *Journal of Geophysical Research* 105:25,791-725,808.
4. Kent DV & Irving E (2010) Influence of inclination error in sedimentary rocks on the Triassic and Jurassic apparent polar wander path for North America and implications for Cordilleran tectonics. *Journal of Geophysical Research* 115:B10103, doi:10110.11029/12009JB007205.
5. Kent DV & Tauxe L (2005) Corrected Late Triassic latitudes for continents adjacent to the North Atlantic. *Science* 307:240–244.
6. Irmis RB, Mundil R, Martz JW, & Parker WG (2011) High-resolution U–Pb ages from the Upper Triassic Chinle Formation (New Mexico, USA) support a diachronous rise of dinosaurs. *Earth and Planetary Science Letters* 309:258-267.
7. Gerstenberger H & Haase G (1997) A highly effective emitter substance for mass spectrometric Pb isotope ratio determinations. *Chemical Geology* 136(3-4):309-312.
8. Mundil R, Ludwig KR, Metcalfe I, & Renne PR (2004) Age and timing of the Permian mass extinctions: U/Pb dating of closed-system zircons. *Science* 305:1760-1763.
9. Black LP*, et al.* (2003) The application of SHRIMP to Phanerozoic geochronology; a critical appraisal of four zircon standards. *Chemical Geology* 200(1-2):171-188.
10. Wotzlaw J-F*, et al.* (2014) Towards accurate numerical calibration of the Late Triassic: High-precision U-Pb geochronology constraints on the duration of the Rhaetian. *Geology* 42(7):571-574.
11. Ramezani J*, et al.* (2011) High-precision U-Pb zircon geochronology of the Late Triassic Chinle Formation, Petrified Forest National Park (Arizona, USA): Temporal constraints on the early evolution of dinosaurs. *Geological Society of America Bulletin* 123(11/12):2142-2159.
12. Atchley SC*, et al.* (2013) A linkage among Pangean tectonism, cyclic alluviation, climate change, and biologic turnover in the Late Triassic: The Record From The Chinle Formation, Southwestern United States. *Journal of Sedimentary Research* 83:1147-1161.
13. Nordt L, Atchley S, & Dworkin S (2015) Collapse of the Late Triassic megamonsoon in western equatorial Pangea, present-day American Southwest. *Geological Society of America Bulletin* 127:1798-1815.
14. Scholz D & Hoffmann DL (2011) StalAge – An algorithm designed for construction of speleothem age models. *Quaternary Geochronology* 6:369–382.
15. Martz JW & Parker WG (2010) Revised Lithostratigraphy of the Sonsela Member (Chinle Formation, Upper Triassic) in the Southern Part of Petrified Forest National Park, Arizona. *PLoS ONE* 5(2):e9329.
16. Olsen PE*, et al.* (2018) Colorado Plateau Coring Project, Phase I (CPCP-I): A continuously cored, globally exportable chronology of Triassic continental environmental change from Western North America. *Scientific Drilling* in review.
17. Kent DV, Olsen PE, & Muttoni G (2017) Astrochronostratigraphic polarity time scale (APTS) for the Late Triassic and Early Jurassic from continental sediments and correlation with standard marine stages. *Earth-Science Reviews* 166:153–180.

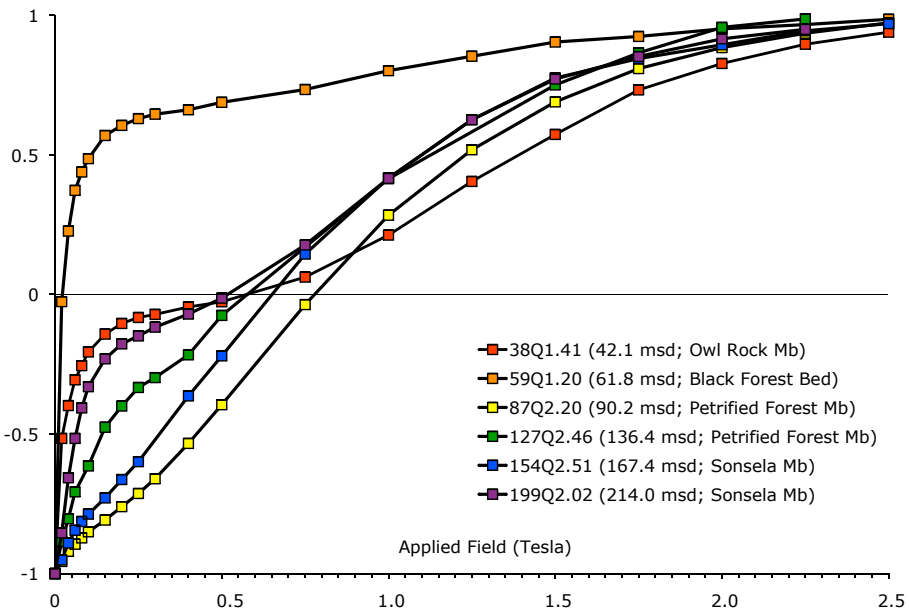

Fig. S1. Normalized backfield isothermal remanent magnetization (IRM) demagnetization curves of representative samples from the upper Chinle Formation (Owl Rock, Petrified Forest and Sonsela members) in core PFNP-1A.

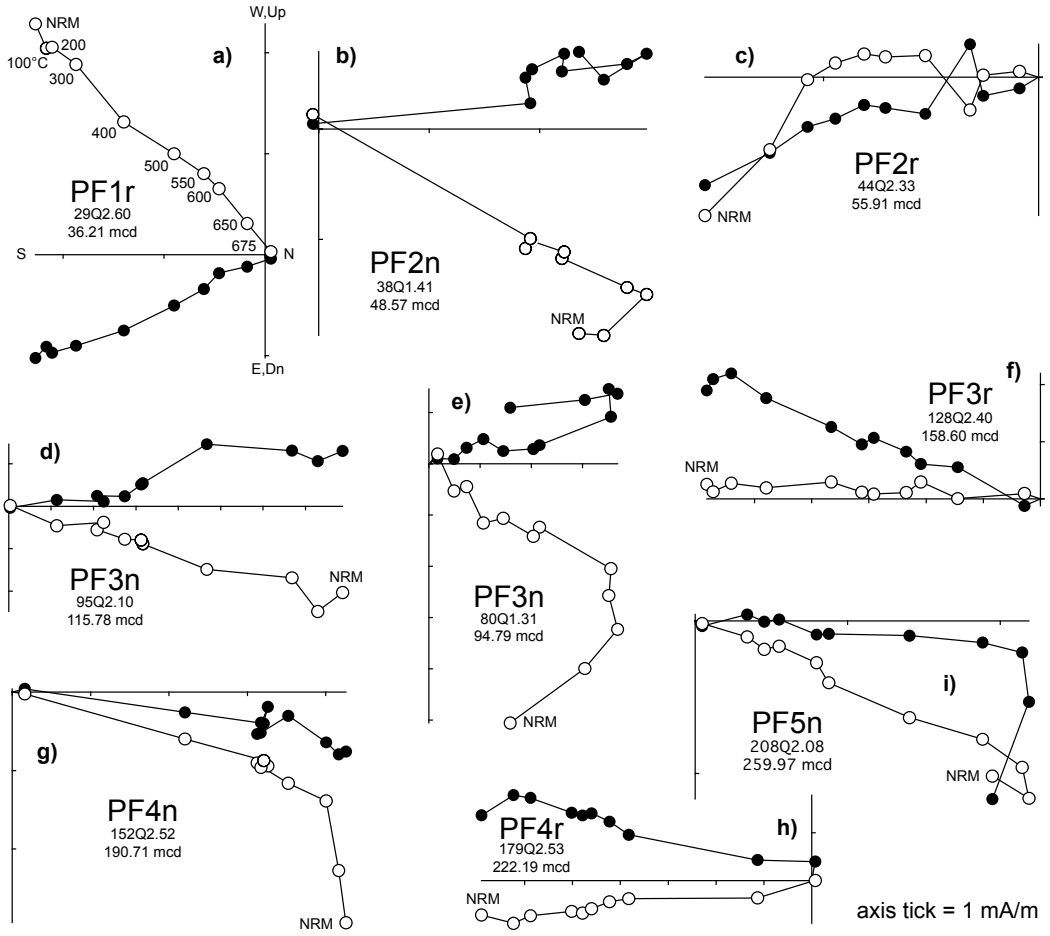

Fig. S2. Vector endpoint demagnetograms of NRM for representative samples from upper Chinle Formation in core PFNP-1A. All plots (a–i) use same convention as for sample in upper left (a) with open/closed symbols on vertical/horizontal orthogonal axes in stratigraphic coordinates (corrected for azimuth and tilt of core hole). NRM is natural remanent magnetization of the sample before stepwise thermally demagnetization with levels in °C as labeled in (a).

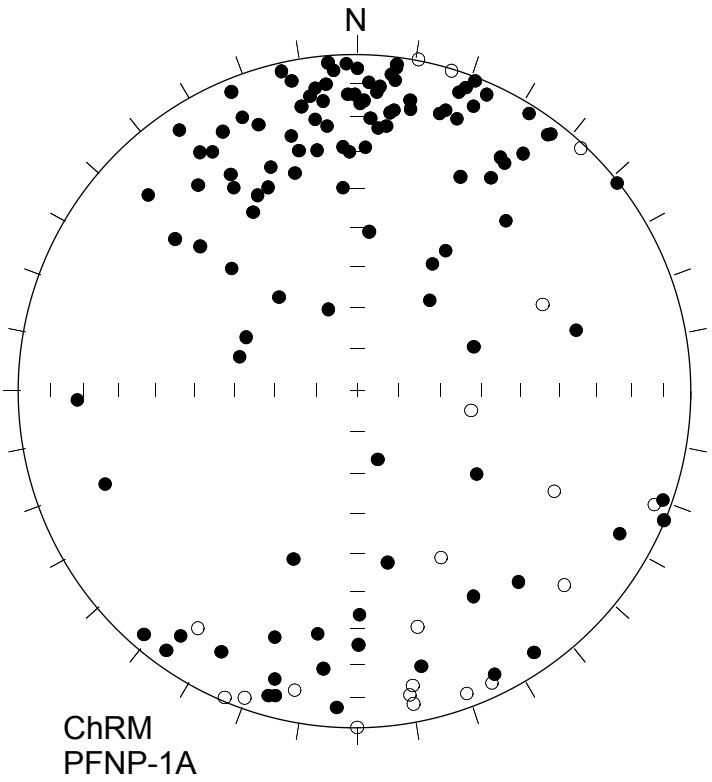

Fig. S3. Equal-area plot (open/closed circles on upper/lower hemisphere) of ChRM directions isolated in 132 samples from upper Chinle Fm. in core PFNP-1A (**Table S3**). The ChRM directions fall into a northerly group interpreted as normal polarity and a southerly group of reverse polarity.

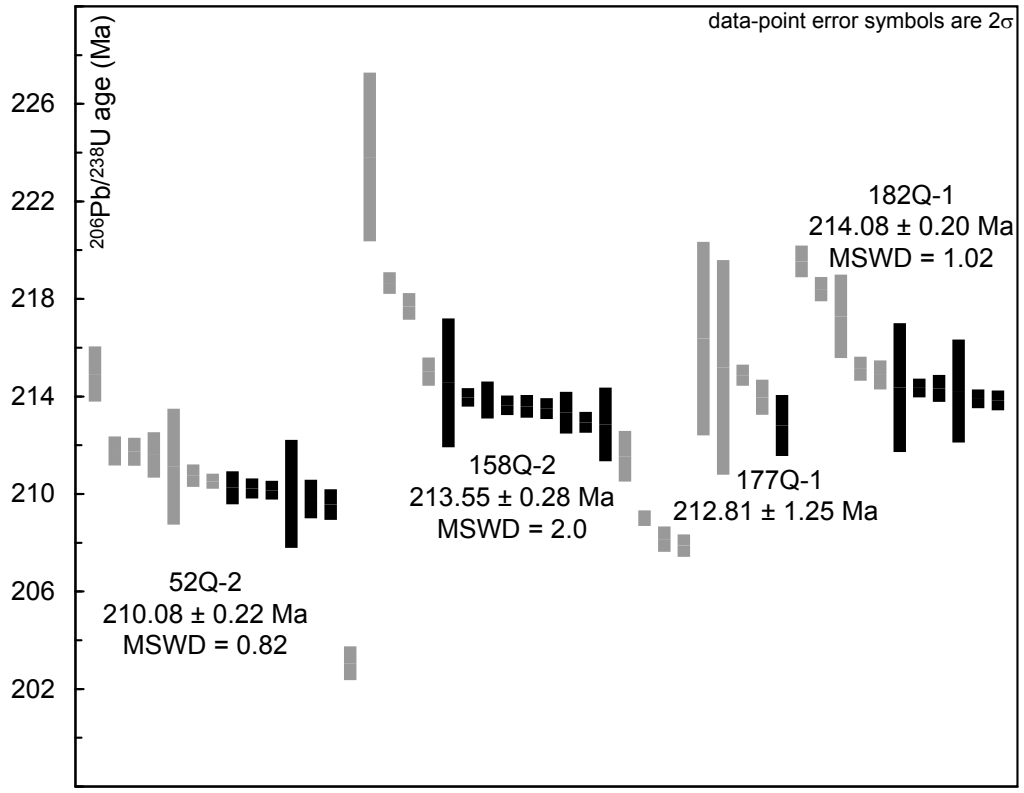

Fig. S4. Individual 206Pb/238U ages of zircon analyses from samples of tuffaceous sandstones in Chinle Fm. from core PFNP-1A (see **Table S4).** Vertical bars show full 2σ uncertainties; zircon analyses with black bars were used to calculate the sample mean age and 2σ uncertainty (95% confidence interval).

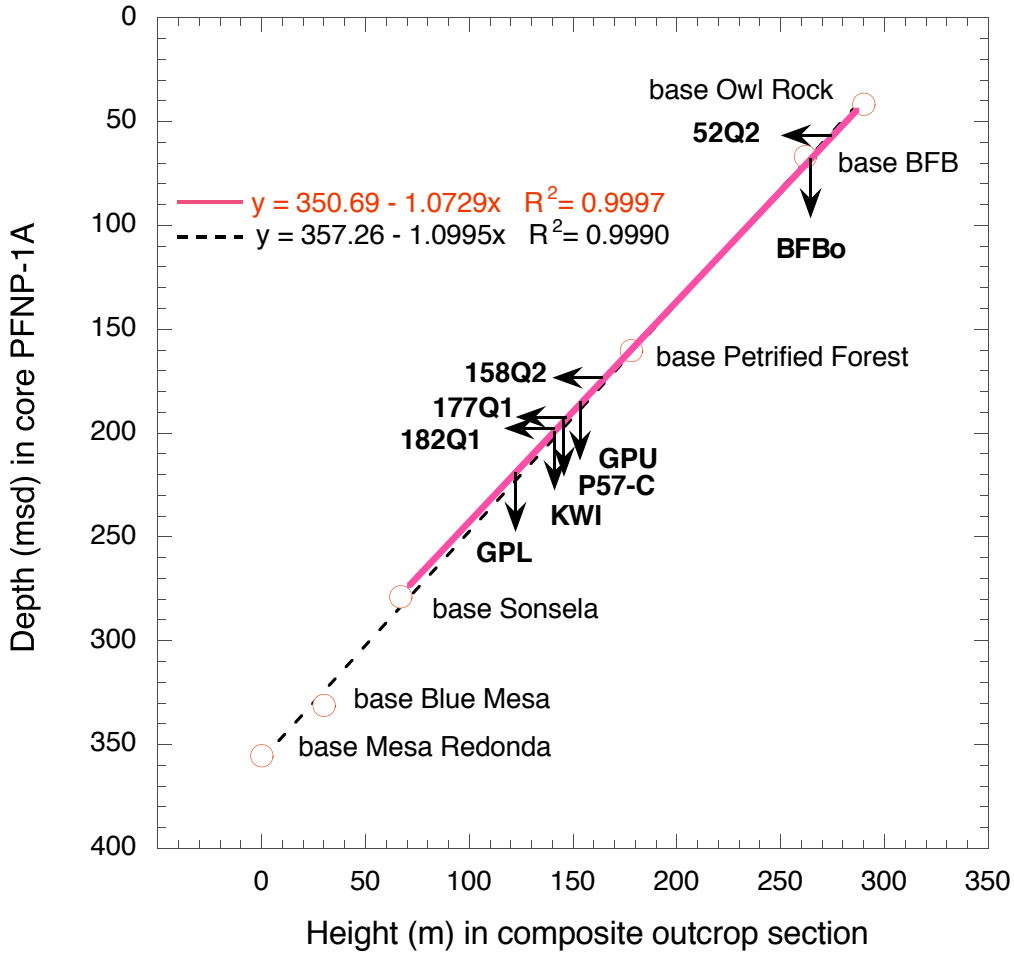

Fig. S5. Stratigraphic heights (circles) of the bases of the Mesa Redonda, Blue Mesa, Sonsela, Petrified Forest and Owl Rock members including the base of the Black Forest Bed (BFB) of the Chinle Fm. identified in a composite outcrop section (11, 12) versus their depth in core PFNP-1A (**Table S1**). Two linear regressions are shown (both equations given), one for all these units (dashed line) and another for just the base of the Sonsela Mb. to the base of the Owl Rock Mb. (solid line), which was used to place the U-Pb CA-TIMS dated zircon samples from outcrop (BFBo, GPU, P57-C, KWI and GPL from (11, 13)) in the same stratigraphic framework as the U-Pb CA-TIMS dated zircon samples from core PFNP-1A (52Q2, 158Q2, 177Q1, and 182Q1 reported here) (**Table S4**).

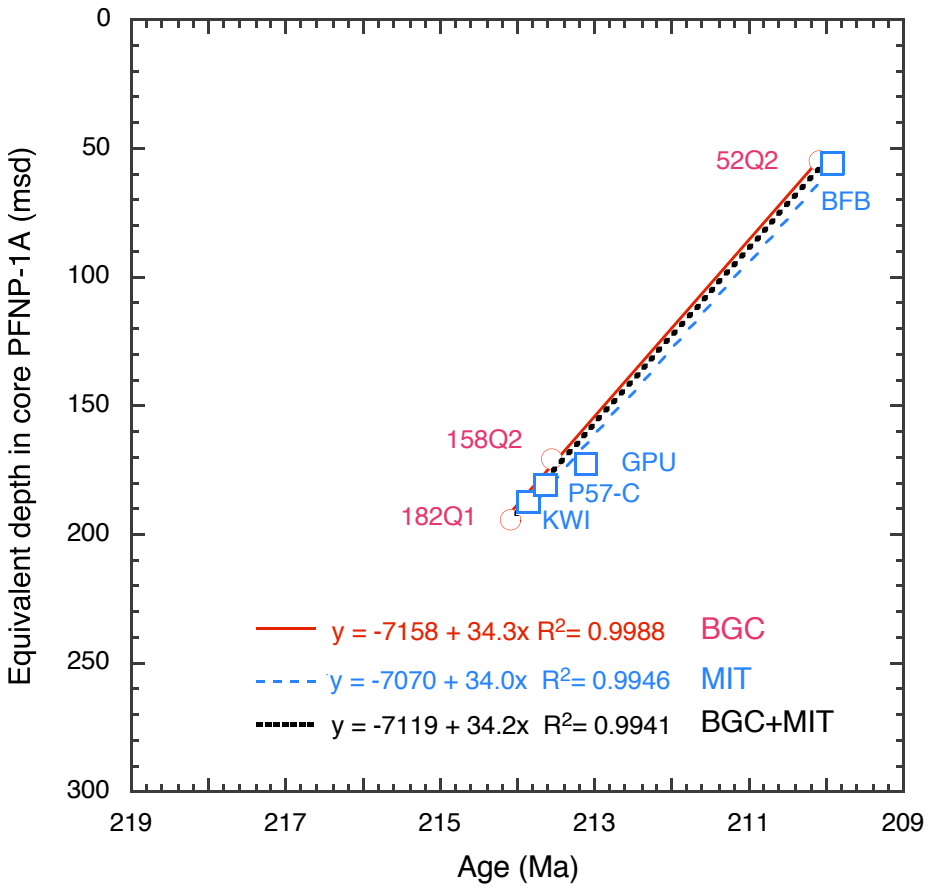

Fig. S6. Stratigraphic distribution of U-Pb CA-TIMS dated zircon samples taken from core PFNP-1A and analyzed by the BGC lab and reported here (circles; sample 177Q1 with large uncertainty of ±1.25 Myr is not plotted) compared to published U-Pb CA-TIMS dated zircon samples taken from outcrop (squares) and analyzed in the MIT lab (11, 13) that were projected into the depth scale of the core using base of the BFB in common (**Table S4**). Linear regressions of depth versus age for both sets of data separately and combined are shown.

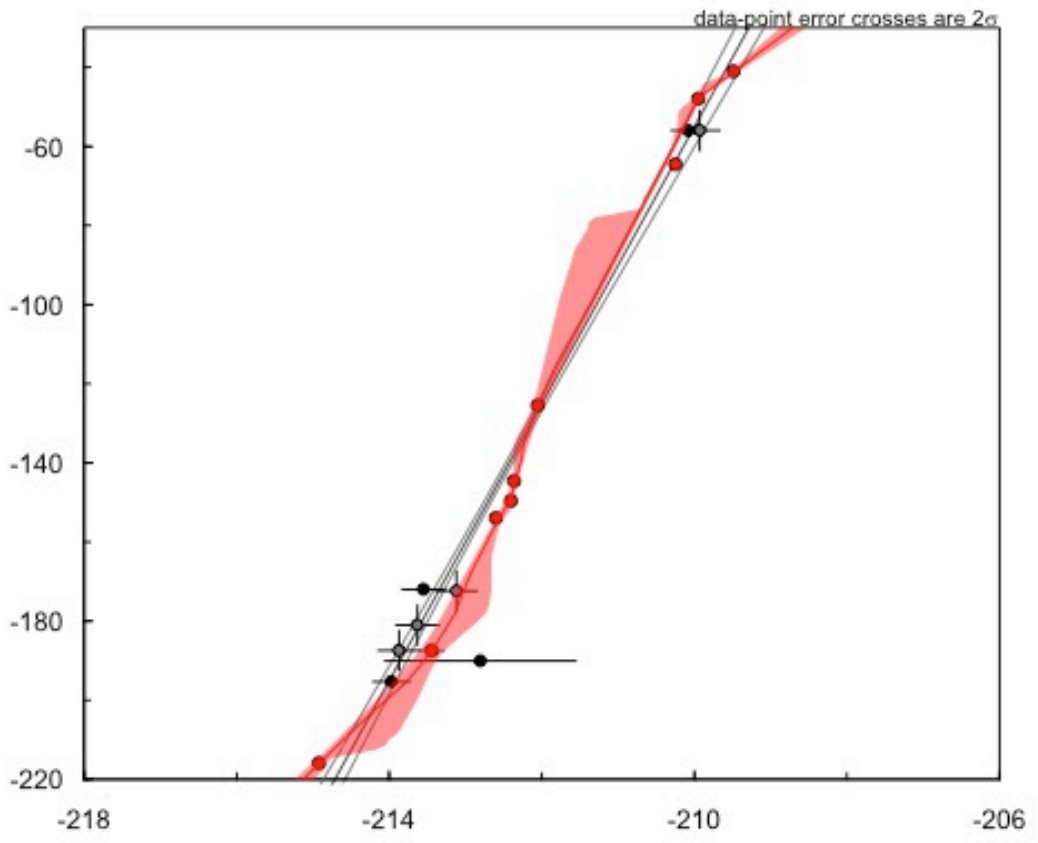

Fig. S7. Stratigraphic distribution of U-Pb CA-TIMS dated samples taken from core PFNP-1A (circles) and published results taken from outcrop (11, 13) that were projected into the common depth scale of the core with an assumed ±5 m stratigraphic uncertainty (squares), all shown with ±2σ age uncertainties (**Table S4**), compared with magnetozone boundaries with their stratigraphic uncertainties in core PFNP-1A as correlated to APTS (**Table S2**). The 95% confidence interval in the depth versus age relationship for the magnetozones using the StalAge algorithm and Monte Carlo technique (14) overlaps for the most part with a linear fit and 95% error envelope through the zircon ages but reveals varying age biases in the populations of redeposited zircons.

Table S1. Lithostratigraphic subdivisions of Chinle Fm. in core PFNP-1A compared to their relative position in a composite outcrop section in and around Petrified Forest National Park.

Rock units[&]	PFNP-1A, msd[#]	Composite height, m*
top (eroded) of Chinle Fm.	20.6	
base Owl Rock Mb.	41.7	290.0
base Black Forest Bed	66.9	262.0
base Petrified Forest Mb.	160.3	178.0
base Sonsela Mb.	278.9	67.0
base Blue Mesa Mb.	331.2	30.0
base Mesa Redonda Mb. (=base Chinle Fm.)	355.4	0.0

[$]Ref. (15). [#]Meters stratigraphic depth for a core hole inclination of 60°; Ref. (16). *Ref. (12).

Table S2. Paleomagnetic polarity zones in core PFNP-1A.

Magneto-zone	Base, mcd	Base, msd	±, msd	Chron	Age, Ma	Ecc_{405}: k
PF1r	47.40	41.05	0.41	E17r	209.49	517.73
PF2n	55.40	47.98	0.44	E17n	209.95	518.87
PF2r	74.49	64.51	2.70	E16r	210.25	519.60
PF3n	144.80	125.40	1.65	E16n	212.05	524.05
PF3r.1r	166.80	144.45	0.55	E15r.2r	212.36	524.82
PF3r.1n	172.60	149.48	1.63	E15r.1n	212.40	524.90
PF3r	177.67	153.87	0.48	E15r	212.60	525.41
PF4n	216.23	187.26	5.16	E15n	213.44	527.47
PF4r	249.10	215.73	1.77	E14r	214.92	531.15
PF5n	>278.01	>240.76		E14n?	216.16	534.19

Magnetozone is the magnetic polarity interval numbered from the uppermost identifiable polarity interval of the Chinle Fm. in this core (PF1r) to the lowermost polarity interval (PF5n) in the part of the core sampled for this study, with a prefix, PF, for Petrified Forest and suffixes n and r for predominantly normal and reverse polarity. The identified base of each magnetozone is designated in mcd, meters core depth, and in msd, meter stratigraphic depth, msd, by taking into account 60° inclination of the core hole; sampling resolution for polarity boundary given as ± msd (**Table S4**). Proposed correlative Chron for each magnetozone is given with its starting Age in million years ago (Ma) and position within a 405 kyr orbital eccentricity cycle (Ecc_{405}:k) where k is the fractional number of predicted cycles counting back from the most recent peak value (k=1) at 0.216 Ma (17). Reliable data for PF1r start in samples only at 38 mcd (~33 msd) above which the results are very scattered due to weathering and drilling disturbance in the porous poorly lithified sediment; the base of PF5n was not reached in this suite of samples.

Table S3. Paleomagnetic results from principal component analysis.

mcd	msd/60°	ID	N	MAD	bDec	bInc	bLon	bLat	rbLon	rbLat	T1	T2	Notes
24.03	20.81	20Q2.44	5	12.7	319.9	60.6	184.2	58.2	218.0	48.9	300	600	
29.28	*25.36*	*24Q1.33*	*5*	*24.5*	*110.0*	*-9.5*	*332.4*	*-19.1*	*343.3*	*-29.5*	*300*	*600*	
29.78	25.79	24Q2.05	5	3.7	100.2	-61.9	14.2	-29.9	26.2	-21.3	300	600	
30.61	26.51	25Q1.13	5	13.7	20.9	2.3	35.8	50.9	359.5	58.7	300	600	
31.75	27.50	25Q2.64	5	3.7	125.2	54.3	292.4	-3.4	295.2	-27.3	300	600	
32.22	27.90	26Q2.06	5	7.5	16.6	15.7	37.0	58.9	347.6	64.5	300	600	
33.34	28.87	27Q1.58	5	8.2	69.7	59.8	312.0	36.2	304.4	15.4	300	600	
33.91	29.37	27Q2.59	5	7.8	155.3	-5.0	290.9	-50.2	317.1	-72.5	300	600	
34.50	29.88	28Q2.18	5	13.2	111.1	-6.2	330.3	-19.0	341.2	-30.3	300	600	
36.21	31.36	29Q2.60	5	3.5	153.4	-43.7	324.8	-65.2	28.1	-67.8	300	600	
36.90	31.96	30Q1.63	5	13.8	118.7	12.3	317.6	-19.2	328.2	-35.4	300	600	
37.39	32.38	30Q2.55	5	3.8	268.0	18.2	169.0	3.7	171.8	8.7	300	600	
38.04	32.94	31Q1.55	5	7.5	249.5	21.4	181.3	-9.8	177.0	-8.9	300	600	
38.64	33.46	31Q2.44	5	10.5	146.0	7.0	296.9	-39.9	315.3	-61.5	300	600	
41.00	*35.51*	*33Q1.62*	*5*	*35.8*	*83.5*	*1.5*	*343.3*	*5.7*	*342.6*	*-2.4*	*300*	*600*	
42.53	*36.83*	*34Q2.51*	*5*	*11.3*	*26.3*	*24.7*	*16.6*	*57.5*	*336.4*	*55.3*	*300*	*600*	*high J?*
42.10	36.46	34Q2.08	5	9.8	200.6	45.6	230.0	-24.9	217.0	-42.5	300	600	
42.93	37.18	34Q3.18	5	9.9	170.0	46.9	260.0	-26.1	255.1	-51.2	300	600	
42.95	37.20	34Q3.20	5	6.9	166.9	17.1	268.5	-44.5	265.5	-70.5	300	600	
43.83	37.96	35Q1.31	5	10.7	163.5	72.5	258.9	3.9	258.0	-21.3	300	600	
44.39	38.44	35Q2.15	4	8.5	139.9	26.6	295.2	-27.9	305.6	-50.6	300	550	
45.20	39.14	36Q1.09	5	11.5	117.2	-34.6	341.5	-32.8	359.7	-37.6	300	600	
45.29	39.22	36Q1.18	4	5.8	215.7	11.3	203.4	-37.2	181.9	-42.5	300	550	
46.10	*39.92*	*36Q2.35*	*5*	*32.2*	*224.2*	*39.0*	*207.0*	*-19.1*	*196.2*	*-28.3*	*300*	*600*	
46.93	40.64	37Q1.30	5	9.0	179.4	33.9	250.9	-36.3	237.7	-59.6	300	600	PF1r
47.06	*40.76*	*37Q1.43*	*5*	*28.2*	*175.4*	*40.7*	*255.2*	*-31.5*	*246.4*	*-55.8*	*300*	*600*	
47.87	41.46	37Q2.48	5	11.9	31.7	20.2	13.0	52.1	340.3	49.9	300	600	PF2n
48.57	42.06	38Q1.41	5	2.0	346.3	27.9	104.9	66.3	207.4	83.9	300	600	
50.57	43.80	39Q2.29	5	11.3	32.3	26.6	7.9	54.1	334.6	49.4	300	600	
51.85	44.90	40Q1.65	5	4.2	51.5	1.8	4.0	31.2	348.8	29.0	300	600	
54.20	46.94	42Q2.10	5	2.5	42.8	-2.8	13.2	35.9	353.8	37.0	300	600	
54.89	47.54	43Q1.03	5	3.3	326.5	16.7	127.3	49.5	160.9	65.9	300	600	PF2n
55.91	48.42	44Q2.33	5	10.4	169.8	-6.2	269.0	-56.6	261.9	-82.4	300	600	PF2r
57.29	*49.62*	*46Q1.14*	*5*	*23.0*	*228.3*	*17.8*	*194.7*	*-26.5*	*180.8*	*-29.5*	*300*	*600*	
60.71	52.58	48Q2.53	5	4.3	198.4	23.8	226.7	-39.4	203.3	-54.2	300	600	
61.40	*53.17*	*50Q2.70*	*5*	*31.6*	*189.9*	*-41.9*	*209.4*	*-76.1*	*124.6*	*-67.4*	*300*	*600*	
62.85	*54.43*	*51Q2.15*	*5*	*35.3*	*197.4*	*-3.1*	*220.6*	*-52.8*	*181.1*	*-62.1*	*300*	*600*	
64.71	*56.04*	*52Q2.45*	*5*	*13.3*	*96.1*	*3.7*	*335.2*	*-3.9*	*339.1*	*-14.6*	*300*	*600*	*zapped*
66.02	*57.18*	*54Q1.19*	*5*	*23.0*	*219.1*	*18.9*	*203.1*	*-31.9*	*185.2*	*-37.9*	*300*	*600*	
66.88	*57.92*	*54Q2.47*	*5*	*25.1*	*74.6*	*4.9*	*347.2*	*14.0*	*342.6*	*6.6*	*300*	*600*	
68.22	*59.08*	*56Q1.25*	*5*	*23.0*	*253.4*	*25.7*	*180.8*	*-5.3*	*178.6*	*-4.6*	*300*	*600*	
68.73	*59.52*	*56Q2.23*	*5*	*30.5*	*285.6*	*31.9*	*166.1*	*22.4*	*178.0*	*26.6*	*300*	*600*	
70.08	*60.61*	*57Q2.47*	*5*	*38.9*	*304.5*	*7.3*	*141.9*	*30.0*	*158.7*	*43.5*	*300*	*600*	
71.37	61.81	59Q1.20	5	8.6	150.6	30.5	283.7	-31.4	290.6	-56.3	300	600	PF2r
72.06	*62.41*	*59Q2.24*	*5*	*21.5*	*116.5*	*-53.1*	*358.1*	*-38.5*	*17.8*	*-35.4*	*300*	*600*	
73.65	*63.78*	*61Q1.44*	*5*	*30.8*	*71.1*	*46.8*	*325.4*	*30.3*	*317.3*	*13.5*	*300*	*600*	
74.25	*64.32*	*63Q1.18*	*5*	*24.3*	*30.8*	*67.2*	*297.1*	*63.2*	*285.8*	*38.8*	*300*	*600*	
75.69	*65.549*	*64Q1.10*	*5*	*32.7*	*351.8*	*32.4*	*95.0*	*71.1*	*261.2*	*83.0*	*300*	*600*	
76.58	*66.32*	*64Q2.28*	*5*	*20.1*	*107.7*	*59.9*	*297.5*	*10.8*	*297.6*	*-12.4*	*300*	*600*	
77.61	67.21	66Q1.35	5	12.2	338.8	30.0	120.5	63.2	190.0	77.1	300	600	PF3n
80.07	69.34	67Q2.67b	5	13.1	346.6	3.4	93.6	54.4	99.4	80.1	300	600	
80.74	69.92	68Q2.05	6	9.8	2.2	9.7	65.8	59.7	10.2	77.4	300	600	

81.60	70.67	69Q1.22	7	11.3	313.0	16.5	139.9	39.5	163.8	52.6	300	600	
85.14	73.73	71Q2.62	6	6.7	336.2	34.8	129.3	63.6	196.5	73.5	300	600	
86.50	74.91	73Q1.22	7	6.8	329.6	26.9	130.5	55.6	175.8	68.9	300	600	
86.83	75.20	73Q2.10	6	3.4	312.4	37.1	154.2	46.0	183.9	51.7	300	600	
89.91	77.86	76Q2.20	6	6.7	18.9	7.6	36.7	54.2	355.6	61.4	300	600	
92.46	80.07	78Q2.13	5	10.3	37.2	5.5	14.9	42.7	350.2	43.4	400	600	
93.85	81.28	79Q2.21	7	6.5	350.5	28.8	96.0	68.5	249.5	85.3	300	600	
94.79	82.09	80Q1.31	6	6.1	344.0	33.6	114.7	68.1	213.9	79.8	300	600	
95.62	82.81	80Q2.37	7	12.6	4.3	51.2	20.9	85.2	282.2	65.4	300	600	
96.40	83.49	81Q2.26	6	8.9	33.1	21.0	10.9	51.4	339.5	48.5	300	600	
97.93	84.81	83Q1.15	7	6.9	20.2	15.5	31.2	57.1	346.8	60.9	300	600	
98.50	85.30	83Q2.22	7	9.9	19.8	5.4	36.2	52.8	357.3	60.2	300	600	
99.90	86.52	84Q2.14	6	8.3	295.4	60.2	187.6	40.0	206.3	32.8	300	600	
103.69	89.80	87Q1.37	7	2.4	332.9	35.5	134.4	61.5	193.3	70.5	300	600	
104.15	90.20	87Q2.20	6	3.6	7.0	8.5	56.7	58.5	4.4	72.8	300	600	
106.88	92.56	89Q1.51	7	7.8	32.4	49.6	340.7	62.5	310.3	46.7	300	600	
107.53	93.12	89Q2.47	7	12.9	354.9	3.1	79.4	56.1	49.8	80.0	300	600	
108.49	93.96	90Q2.15	6	2.2	7.0	3.3	57.6	55.9	12.1	71.6	300	600	
110.62	95.80	92Q1.14	7	13.7	340.4	69.4	218.7	67.3	244.7	46.8	300	600	
112.11	*97.09*	*93Q1.10*	*6*	*20.4*	*356.2*	*4.2*	*77.2*	*56.8*	*41.7*	*79.9*	*300*	*600*	
113.17	98.008	93Q2.40	7	9.7	35.1	15.6	12.0	47.9	343.5	46.3	300	600	
114.39	*99.07*	*94Q2.56*	*6*	*22.8*	*3.2*	*33.5*	*59.8*	*73.0*	*309.8*	*75.8*	*300*	*600*	
115.78	100.27	95Q2.10	7	4.2	348.9	15.6	93.4	61.0	109.5	86.7	300	600	
116.90	101.24	96Q1.22	6	6.8	356.0	39.8	86.9	77.0	275.5	77.1	300	600	
117.43	*101.70*	*97Q1.09*	*7*	*21.4*	*165.4*	*9.3*	*272.2*	*-47.9*	*273.6*	*-73.7*	*300*	*600*	
120.02	103.94	99Q1.09	6	5.3	358.2	30.2	75.5	71.1	305.1	81.0	300	600	
121.16	104.93	100Q2.06	7	11.0	3.8	12.6	62.4	61.1	1.3	76.5	300	600	
123.05	106.56	101Q2.62a	6	6.8	329.7	38.9	142.0	60.5	195.6	66.8	300	600	
123.54	106.99	102Q1.10	6	14.3	1.4	15.4	67.2	62.7	358.1	79.2	400	600	
125.17	*108.40*	*103Q1.51*	*6*	*27.6*	*44.5*	*-0.8*	*10.9*	*35.4*	*352.1*	*35.6*	*300*	*600*	
125.82	108.96	103Q3.11	7	15.9	314.0	47.1	163.5	50.6	196.2	51.3	300	600	
127.44	*110.37*	*104Q2.58*	*6*	*25.5*	*101.2*	*69.2*	*289.7*	*21.2*	*288.5*	*-3.4*	*300*	*600*	
128.03	*110.88*	*105Q1.33*	*7*	*17.5*	*303.0*	*81.3*	*230.6*	*42.9*	*240.3*	*21.7*	*300*	*600*	
128.43	*111.22*	*105Q2.05*	*6*	*31.0*	*338.6*	*33.6*	*124.4*	*64.7*	*198.3*	*75.9*	*300*	*600*	
129.69	112.31	106Q1.46	7	7.7	31.9	4.1	21.2	45.6	352.9	48.4	300	600	
131.44	113.83	107Q2.02	6	6.6	2.8	20.5	63.6	65.4	343.1	78.3	300	600	
133.14	115.30	108Q2.10	7	5.6	309.6	30.6	151.0	41.5	176.8	49.5	300	600	
134.00	116.05	109Q1.20	6	5.4	358.2	13.4	74.0	61.7	11.4	81.8	300	600	
134.68	116.64	109Q2.15	7	5.8	337.1	4.7	108.3	51.0	133.5	74.0	300	600	
		110Q2.13	*6*	*3.8*	*353.3*	*15.0*	*84.4*	*61.9*	*35.3*	*86.1*	*300*	*600*	*ID?*
137.04	118.68	112Q2.05	7	3.9	16.5	-1.6	43.4	50.9	6.5	62.0	300	600	
139.42	120.74	114Q1.06	6	5.9	2.0	28.9	64.5	70.3	318.9	78.2	300	600	
140.10	121.33	114Q2.22	7	4.4	6.2	6.7	58.5	57.8	8.4	73.1	300	600	
141.24	122.32	115Q2.40	6	4.6	10.8	16.5	47.3	61.6	348.6	70.2	300	600	
142.89	123.75	116Q2.59	7	16.2	10.4	13.8	49.0	60.3	353.0	70.4	300	600	PF3n
143.83	*124.56*	*118Q1.12*	*6*	*23.2*	*289.9*	*49.1*	*176.6*	*31.9*	*192.5*	*30.4*	*300*	*600*	
146.70	127.05	120Q2.23	7	15.0	189.2	27.7	238.6	-39.4	217.9	-58.8	300	600	PF3r.1r
147.80	128.00	121Q1.28	6	4.3	195.0	7.0	227.1	-48.9	193.1	-62.1	300	600	
150.00	129.90	122Q2.20	6	2.2	4.3	10.9	61.6	60.1	4.0	75.7	300	600	
153.00	132.50	124Q2.01	6	9.0	183.7	6.4	244.3	-51.5	210.5	-71.1	300	600	
154.43	133.74	125Q2.33	3	12.7	169.3	-11.9	271.4	-59.3	272.4	-85.1	500	600	
155.75	134.88	126Q2.20	6	4.4	191.8	-10.1	227.5	-58.1	177.3	-68.5	300	600	
156.98	135.95	127Q1.63	7	14.6	186.9	18.0	240.5	-45.2	214.5	-64.5	300	600	
157.51	136.41	127Q2.46	6	5.0	207.4	13.7	213.2	-40.7	188.1	-49.6	300	600	
158.60	137.35	128Q2.40	7	2.2	200.1	-3.3	216.5	-51.7	179.1	-59.6	300	600	
159.87	138.45	129Q2.60	6	2.8	180.0	-0.1	250.2	-55.0	212.7	-76.0	300	600	
161.25	*139.65*	*130Q2.55*	*7*	*29.4*	*186.6*	*48.0*	*243.8*	*-25.6*	*233.3*	*-47.5*	*300*	*600*	

162.49	140.72	131Q2.35	6	4.6	179.7	25.5	250.6	-41.5	233.6	-64.4	300	600
163.34	141.46	132Q1.28	7	14.5	195.9	12.0	227.0	-46.2	196.6	-60.0	300	600
166.16	143.90	134Q1.05	6	11.7	170.2	-9.2	269.0	-58.2	260.1	-83.9	300	600 PF3r.1r
167.43	145.00	135Q1.10	7	15.6	39.1	62.1	312.8	58.9	296.7	37.1	300	600 PF3r.1n
170.72	147.85	137Q1.35	6	13.7	41.4	33.7	353.7	49.8	328.6	40.6	500	600 PF3r.1n
174.47	151.10	139Q2.34	7	13.3	133.3	-16.8	319.8	-39.8	344.0	-52.9	300	600 PF3r
176.87	153.17	141Q2.31	3	15.8	221.1	4.3	195.4	-36.5	175.3	-38.4	300	500
177.12	153.39	141Q2.56	5	10.6	160.1	-4.9	284.2	-52.5	307.1	-76.5	500	600 PF3r
177.39	*153.62*	*142Q1.01*	*6*	*35.6*	*249.8*	*26.1*	*183.2*	*-7.9*	*179.6*	*-8.0*	*300*	*600*
178.21	154.33	142Q2.67	5	8.8	322.2	24.2	136.4	49.2	170.8	61.9	550	675 PF4n
179.93	*155.82*	*144Q1.11*	*6*	*28.3*	*278.3*	*32.5*	*170.4*	*16.7*	*178.9*	*19.7*	*300*	*600*
181.83	157.47	145Q1.48	7	7.5	0.6	16.3	68.9	63.2	356.7	80.1	300	600
184.58	159.85	147Q1.18	7	11.6	6.8	18.4	55.0	63.6	346.9	74.3	300	600
185.69	160.81	148Q2.47	6	14.9	345.4	23.4	103.8	63.6	180.4	84.4	300	600
186.46	161.48	149Q1.48	7	7.7	332.5	14.9	119.2	52.7	155.7	71.6	300	600
187.02	161.96	149Q2.34	6	4.9	7.0	4.4	57.5	56.5	10.6	71.9	300	600
188.64	163.37	150Q3.59	4	8.9	10.5	-0.5	52.4	53.3	11.8	67.6	300	600
189.11	163.77	151Q1.30	6	14.4	216.2	4.9	200.4	-39.4	177.5	-43.0	300	600
190.71	165.16	152Q2.52	7	2.5	7.5	17.6	53.7	63.0	348.1	73.5	300	600
191.67	*165.99*	*153Q2.29*	*6*	*19.6*	*153.8*	*-30.2*	*308.0*	*-59.9*	*4.2*	*-72.5*	*300*	*600*
193.28	167.39	154Q2.51	7	2.4	358.1	3.8	73.7	56.8	34.0	78.7	300	600
199.71	172.95	160Q1.08	6	4.8	23.7	5.0	30.9	50.7	355.6	56.4	300	600
200.93	*174.01*	*161Q2.16*	*7*	*32.7*	*27.5*	*27.7*	*12.8*	*58.0*	*333.4*	*54.1*	*300*	*600*
203.91	*176.59*	*165Q1.47a*	*6*	*30.8*	*350.7*	*0.6*	*86.2*	*54.1*	*74.8*	*79.6*	*300*	*600*
203.91	176.59	165Q1.47b	5	10.9	355.8	5.7	78.0	57.5	41.4	80.8	300	600
205.09	177.61	166Q2.63	7	12.4	6.3	22.5	54.9	65.9	338.4	74.8	300	600
206.15	178.53	167Q1.72	5	11.5	356.7	28.7	79.5	70.0	304.0	82.7	300	600
206.48	*178.82*	*167Q2.30*	*6*	*38.6*	*326.8*	*6.5*	*121.8*	*45.7*	*148.4*	*65.0*	*300*	*600*
207.20	179.44	168Q1.25	4	5.9	352.1	10.8	85.8	59.5	60.6	84.6	200	500
208.12	*180.24*	*168Q2.46*	*7*	*44.1*	*217.0*	*4.7*	*199.5*	*-39.0*	*177.0*	*-42.3*	*300*	*600*
208.48	*180.55*	*169Q1.01*	*6*	*34.4*	*305.7*	*31.6*	*154.3*	*38.7*	*177.5*	*45.8*	*300*	*600*
208.89	*180.90*	*169Q1.42*	*5*	*32.0*	*315.0*	*29.1*	*146.0*	*45.4*	*175.7*	*54.8*	*300*	*600*
209.18	181.16	169Q2.17	5	14.1	348.0	7.2	92.4	56.6	96.0	82.4	300	600
209.31	181.27	169Q3.06	7	46.0	314.8	21.4	141.2	42.6	168.0	54.6	300	600
210.27	182.10	170Q1.27	3	5.6	25.9	30.5	12.5	60.3	330.3	55.5	550	625 PF4n
211.30	182.99	170Q2.62	5	28.5	190.6	46.9	239.8	-26.0	228.1	-46.8	300	600
212.16	183.74	171Q1.64	6	13.2	74.8	33.2	333.3	22.5	326.9	9.0	300	600 ?
222.19	192.42	179Q2.53	5	0.7	196.2	6.4	225.2	-48.8	191.3	-61.2	300	600 PF4r
222.69	192.86	180Q1.20	5	3.7	17.6	14.2	36.0	57.8	349.0	63.4	300	600
223.56	193.61	180Q2.40	5	10.1	113.0	1.4	325.9	-18.2	336.4	-31.4	300	600
223.80	193.82	180Q2.64	3	8.3	109.8	4.2	326.8	-14.8	335.7	-27.9	625	675
224.49	194.41	181Q1.47	3	7.8	154.2	7.2	287.6	-44.3	304.0	-68.1	625	675
224.87	194.74	181Q2.26	3	10.7	165.7	-28.4	286.5	-66.3	25.9	-83.3	625	675
236.63	204.93	191Q1.42	3	14.9	203.3	-1.0	213.0	-49.2	179.2	-56.2	500	600
247.06	213.96	199Q2.02	2	7.7	213.8	-16.2	193.0	-49.1	163.2	-47.6	500	550 PF4r
251.14	217.49	201Q2.49	5	14.2	65.3	-39.3	12.5	5.7	9.0	10.0	300	600 PF5n
252.04	218.27	202Q2.10	5	5.7	30.9	54.2	332.0	64.8	303.8	46.4	300	600
253.62	219.64	203Q2.25	5	9.8	22.3	10.1	30.6	53.6	351.5	58.4	300	600
254.52	220.42	204Q1.33	5	5.8	353.5	22.4	85.9	65.8	322.8	87.2	300	600
255.58	221.34	204Q2.63	5	7.6	328.7	18.6	126.0	51.7	162.9	68.2	300	600
256.29	221.95	205Q1.58	5	2.9	354.2	9.9	81.6	59.4	43.4	83.4	300	600
256.58	222.20	205Q2.25	5	4.5	350.9	13.0	88.7	60.3	73.4	85.9	300	600
257.54	223.04	206Q1.30	5	6.2	285.7	60.4	190.6	33.1	204.8	25.6	300	600
257.98	*223.42*	*207Q1.13*	*5*	*5.9*	*166.7*	*-48.3*	*316.7*	*-77.4*	*62.6*	*-71.0*	*300*	*600 zapped?*
258.61	223.96	207Q2.38	6	11.5	337.1	13.5	112.3	54.8	149.3	75.9	200	625
259.91	225.09	208Q1.54	5	3.8	0.1	5.3	70.0	57.6	24.4	77.8	300	600
259.97	225.14	208Q2.08	5	2.3	4.6	23.3	58.8	66.7	336.2	76.5	300	600

262.29	227.15	210Q1.17	5	3.8	36.8	6.3	14.9	43.3	349.8	43.8	300	600
263.03	227.79	210Q2.16	5	3.2	359.6	13.6	71.0	61.8	6.7	80.6	300	600
268.53	*232.55*	*214Q1.32*	*5*	*39.9*	*336.3*	*45.0*	*143.9*	*68.0*	*215.0*	*69.0*	*300*	*600*
269.93	233.77	215Q1.20	5	12.1	325.6	7.5	123.5	45.4	150.3	64.0	300	600
271.66	*235.26*	*216Q1.40*	*5*	*25.0*	*293.8*	*35.1*	*163.7*	*30.1*	*180.1*	*34.4*	*300*	*600*
272.10	235.65	216Q2.20	5	14.6	339.6	17.3	110.5	57.8	155.5	78.7	300	625
274.35	237.59	219Q2.07	5	9.6	328.6	30.5	134.6	56.3	181.2	67.6	300	600
278.01	240.76	221Q2.27	5	8.5	351.2	20.1	90.3	64.0	26.1	89.6	300	600

mcd is meters core depth and msd is meters stratigraphic depth of samples (ID) taken in core PFNP-1A that was deviated by 60° from horizontal toward azimuth of 135° in flat-lying strata. N is number of steps between demagnetization temperatures T1 and T2 (°C) used to calculate best-fit magnetization vector described by its maximum angular deviation (MAD), the declination (bDec) and inclination (bInc) in bedding coordinates whose virtual geomagnetic pole is located at longitude (bLon) and latitude (bLat) with respect to present-day coordinates and rotated longitude (rbLon) and latitude (rbLat) with respect to a mean Late Triassic paleomagnetic reference pole for North America (4). Data in italicized red font were rejected for magnetostratigraphic interpretation of polarity; samples with valid data from the tops and bottoms of magnetozones are identified in Notes.

Table S4. U-Pb CA-TIMS zircon dates in upper Chinle Fm.

ID	Unit	mcd	msd	Age Ma	±2s Myr	Ref.
Core PFNP-1A						
52Q2	BFB	64.6	56.0	210.08	0.22	1
158Q2	Sonsela	198.6	172.0	213.55	0.28	1
177Q1	Sonsela	219.4	190.0	212.81	1.25	1
182Q1	Sonsela	225.5	195.3	214.08	0.20	1
Outcrop projected to core PFNP-1A						
BFBo	BFB		56.0	209.93	0.07	2
GPU	Sonsela		172.4	213.12	0.07	2
P57-C	Sonsela		181.0	213.63	0.13	3
KWI	Sonsela		187.4	213.87	0.08	2
GPL	Sonsela		207.8	218.02	0.09	2

Samples (ID) are from lithostratigraphic units in the Chinle Fm. (BFB is Black Forest Bed within the Petrified Forest Mb and Sonsela is Sonsela Mb). Sample levels are in meters core depth (mcd) and meters stratigraphic depth (msd) by accounting for 60° core hole inclination and assuming flat lying strata. The msd for each outcrop sample was projected to core PFNP-1A by correlation of the lithostratigraphy of the measured cumulative section (11, 12) (**Fig. S5**) and registration of the base of the distinctive BFB in outcrop to its equivalent depth in the core. Ref.: 1, This paper; 2, Ref. (11); 3, Ref. (13).

Table S5. Isotopic ratios and ages.

Sample	Pb_c (pg)	Th U	isotopic ratios $^{206}Pb/^{204}Pb$	$^{206}Pb/^{204}Pb$	2σ %er	$^{207}Pb/^{235}U$	2σ %er	$^{206}Pb/^{238}U$	2σ %er	ρ	isotopic age in (Ma) $^{206}Pb/^{238}U$	
52Q-2.Sp61*	7.2	0.71	114	0.05024	5.22	0.2347	5.46	0.033901	0.54	.49	214.92	± 1.13
52Q-2.Sp314*	1.1	0.51	1242	0.05043	0.54	0.2321	0.65	0.033396	0.29	.56	211.77	± 0.60
52Q-2.Sp115*	1.2	0.99	244	0.05055	2.35	0.2326	2.46	0.033390	0.28	.44	211.73	± 0.57
52Q-2.Sp141*	1.0	1.29	140	0.05026	4.63	0.2311	4.84	0.033370	0.45	.52	211.60	± 0.93
52Q-2.Sp86*	2.1	1.69	61	0.05151	11.39	0.2364	11.90	0.033292	1.14	.49	211.12	± 2.38
52Q-2.Sp201*	0.9	1.65	886	0.05033	0.67	0.2305	0.75	0.033232	0.22	.49	210.75	± 0.46
52Q-2.Sp52*	1.1	0.83	631	0.05054	1.01	0.2312	1.07	0.033197	0.15	.44	210.52	± 0.31
52Q-2.Sp57*	1.2	1.51	247	0.05009	2.38	0.2289	2.50	0.033153	0.33	.42	210.25	± 0.68
52Q-2.Sp108*	0.8	0.59	401	0.04979	1.58	0.2274	1.67	0.033148	0.20	.51	210.22	± 0.41
52Q-2.Sp155*	1.0	0.38	422	0.05060	1.36	0.2311	1.43	0.033137	0.18	.44	210.15	± 0.38
52Q-2.Sp310*	2.0	1.60	63	0.05220	10.69	0.2382	11.17	0.033113	1.07	.49	210.00	± 2.22
52Q-2.Sp204*	1.2	1.25	201	0.04900	3.30	0.2234	3.46	0.033080	0.38	.47	209.80	± 0.79
52Q-2.Sp221*	0.8	1.82	233	0.05017	2.84	0.2285	2.98	0.033043	0.30	.50	209.57	± 0.62
52Q-2.Sp20*	0.9	1.97	234	0.05020	2.66	0.2214	2.81	0.032001	0.35	.46	203.06	± 0.69
158Q-2.Sp60*	3.9	1.50	49	0.05598	14.30	0.2726	14.99	0.035330	1.57	.49	223.82	± 3.46
158Q-2.Sp157*	2.7	1.34	546	0.05069	1.12	0.2410	1.20	0.034500	0.21	.43	218.65	± 0.45
158Q-2.Sp163*	2.7	0.99	1711	0.05038	0.47	0.2385	0.57	0.034346	0.26	.59	217.69	± 0.55
158Q-2.Sp161*	4.7	0.76	341	0.05046	1.80	0.2359	1.91	0.033917	0.27	.45	215.01	± 0.58
158Q-2.Sp181*	4.6	1.41	108	0.04928	11.95	0.2299	12.73	0.033843	1.25	.66	214.56	± 2.64
158Q-2.Sp240*	1.4	1.01	1749	0.05054	0.39	0.2351	0.47	0.033748	0.18	.58	213.96	± 0.38
158Q-2.Sp236*	2.7	1.43	256	0.05114	3.24	0.2377	3.40	0.033730	0.36	.50	213.85	± 0.76
158Q-2.Sp262*	1.2	0.90	1167	0.05018	0.68	0.2330	0.73	0.033696	0.19	.39	213.64	± 0.40
158Q-2.Sp15*	2.0	0.99	370	0.05070	1.52	0.2354	1.60	0.033689	0.22	.42	213.59	± 0.47
158Q-2.Sp93*	1.0	1.36	677	0.05039	0.79	0.2338	0.86	0.033674	0.21	.43	213.50	± 0.43
158Q-2.Sp120*	3.7	1.26	146	0.05062	3.91	0.2347	4.09	0.033647	0.41	.48	213.33	± 0.86
158Q-2.Sp142*	1.4	0.70	1460	0.05064	0.41	0.2344	0.48	0.033583	0.20	.52	212.93	± 0.43
158Q-2.Sp18*	1.3	1.65	127	0.04978	6.86	0.2303	7.24	0.033570	0.72	.57	212.85	± 1.51
158Q-2.Sp233*	1.4	1.34	239	0.04950	4.21	0.2276	4.45	0.033361	0.50	.53	211.55	± 1.04
158Q-2.Sp168*	1.4	1.45	864	0.05058	0.66	0.2297	0.72	0.032954	0.15	.45	209.01	± 0.32
158Q-2.Sp276*	1.1	1.66	1005	0.05015	0.88	0.2268	0.96	0.032816	0.25	.43	208.15	± 0.52
158Q-2.Sp55*	1.7	1.56	686	0.05055	1.18	0.2283	1.26	0.032774	0.23	.43	207.88	± 0.46
177Q-1.Sp181	1.2	1.85	47	0.06067	16.42	0.2856	17.21	0.034134	1.83	.47	216.37	± 3.97
177Q-1.Sp120	1.3	0.71	42	0.05587	19.37	0.2616	20.31	0.033945	2.05	.50	215.19	± 4.40
177Q-1.Sp168	1.2	0.76	445	0.05049	1.37	0.2360	1.44	0.033893	0.20	.42	214.87	± 0.43
177Q-1.Sp108	3.1	0.64	241	0.05066	2.29	0.2357	2.40	0.033748	0.34	.40	213.97	± 0.72
177Q-1.Sp81	1.9	0.76	110	0.05144	5.88	0.2380	6.16	0.033562	0.59	.52	212.81	± 1.25
182Q-1.Sp216	1.6	0.86	194	0.05180	2.86	0.2474	2.98	0.034643	0.30	.45	219.54	± 0.65
182Q-1.Sp273	1.1	0.82	1461	0.05055	0.37	0.2402	0.45	0.034460	0.23	.57	218.40	± 0.50
182Q-1.Sp283	0.6	1.30	439	0.05332	4.03	0.2520	4.35	0.034281	0.79	.48	217.29	± 1.71
182Q-1.Sp269	0.9	1.99	1321	0.05036	0.98	0.2357	1.01	0.033936	0.23	.27	215.14	± 0.50
182Q-1.Sp5	1.1	0.97	574	0.05041	0.91	0.2356	0.99	0.033895	0.28	.40	214.88	± 0.60
182Q-1.Sp266	2.1	0.84	1121	0.05039	0.52	0.2349	1.35	0.033813	1.23	.92	214.37	± 2.64
182Q-1.Sp263	0.7	0.49	1412	0.05026	0.53	0.2343	0.58	0.033810	0.18	.41	214.35	± 0.38
182Q-1.Sp197	0.7	1.05	2330	0.05055	0.34	0.2356	0.45	0.033806	0.26	.64	214.33	± 0.55
182Q-1.Sp241	2.0	0.55	72	0.05349	10.70	0.2492	11.25	0.033789	0.99	.58	214.22	± 2.11
182Q-1.Sp265	0.5	0.52	2178	0.05012	0.35	0.2332	0.41	0.033738	0.18	.54	213.90	± 0.39
182Q-1.Sp182	0.6	0.92	3652	0.05038	0.45	0.2343	0.50	0.033728	0.19	.45	213.84	± 0.41

Pb blank composition is $^{206}Pb/^{204}Pb$ = 18.40 ± 0.64, $^{207}Pb/^{204}Pb$ = 15.64 ± 0.25, $^{208}Pb/^{204}Pb$ = 38.04 ± 0.75, and a $^{206}Pb/^{204}Pb$–$^{207}Pb/^{204}Pb$ correlation of +0.47.
Present day Th/U ratio is calculated from radiogenic $^{208}Pb/^{206}Pb$ and age.
Isotopic ratios corrected for mass fractionation (0.15 ± 0.06%/amu), tracer contribution and common Pb contribution (the latter for all ratios but $^{206}Pb/^{204}Pb$).
ρ is correlation coefficient of radiogenic $^{207}Pb/^{235}U$ versus $^{206}Pb/^{238}U$.
Analyses of aliquotes are printed in grey.
Uncertainties of individual ratios and ages are given at the 2σ level and do not include decay constant errors.
Samples denoted with an * were analyzed using the Earthtime 535 tracer solution.
Deficient radiogenic ^{206}Pb due to initial deficit of ^{230}Th is accounted for by assuming a partition coefficient ratio DTh/DU of 0.2 (as applied in Wotzlaw et al., 2014).
Initial deficit of ^{230}Th for zircons analyzed using ET535 is corrected assuming Th/U=3.5 in the magma.